Surface Energy of Nanostructural Materials with Negative Curvature and Related Size Effects

G. Ouyang,[†,‡] C. X. Wang,[‡] and G. W. Yang*[,‡]

Key Laboratory of Low-Dimensional Quantum Structures and Quantum Control of Ministry of Education, and Department of Physics, Hunan Normal University, Changsha 410081, Hunan, P. R. China, and State Key Laboratory of Optoelectronic Materials and Technologies, Institute of Optoelectronic and Functional Composite Materials, Nanotechnology Research Center, School of Physics Science & Engineering, Zhongshan University, Guangzhou 510275, Guangdong, P. R. China

Received February 11, 2009

Contents

1. Introduction 4221
2. Surface Energy of Nanostructures with Negative Curvature 4222
   2.1. Overview 4222
   2.2. Fundamental Aspects 4223
      2.2.1. Classical Approach 4223
      2.2.2. Nanothermodynamics 4224
3. Surface Energy of Nanocavity 4225
   3.1. Background 4225
   3.2. Thermodynamic Analytic Expression of Surface Energy 4226
   3.3. Size Effects Induced by Surface Energy 4227
   3.4. Nonlinear Shrinkage 4228
      3.4.1. Observations 4228
      3.4.2. Kinetic Behaviors 4229
   3.5. Phase Transition: Superheating 4229
   3.6. Sink Effect 4231
      3.6.1. Observations 4231
      3.6.2. Nucleation Thermodynamics in Nanocavities 4231
      3.6.3. Diffusion Kinetics Considerations 4232
   3.7. Summary 4233
4. Surface Energy of Nanotubes 4234
   4.1. Background 4234
   4.2. Thermodynamic Analytic Expression of Inner and Outer Surface Energies 4234
   4.3. Novel Mechanical Behaviors Induced by Surface Energy 4235
   4.4. Mechanical Properties of Nanoporous Structural Materials 4237
   4.5. Summary 4239
5. Surface Energy of Shell−Core Nanostructures 4240
   5.1. Observations 4240
   5.2. Thermodynamic Analytic Expression of Shell−Core Nanostructures 4241
   5.3. Spontaneous Interfacial Alloying 4241
   5.4. Kinetic Considerations 4242
   5.5. Au/Ag Bimetallic System 4243
   5.6. Summary 4243
6. Concluding Remarks 4244
7. Acknowledgments 4244
8. References 4245

* Corresponding author. Tel.: +86-20-8411-3692. Fax: +86-20-8411-3692. E-mail: stsygw@mail.sysu.edu.cn.
† Hunan Normal University.
‡ Zhongshan University.

1. Introduction

As a bridge spanning the gap between the atomistic level and its bulk counterpart, nanoscaled systems have recently become an active area of research in materials science, condensed matter physics, and chemistry because of their unique performance from the fundamental scientific point of view. Of the anomalous physical and chemical properties of nanoscaled systems as compared with those of the bulk material, the high ratio of surface-to-volume is the most striking. The surface or interface effect plays the dominant role in the mechanical, thermal, optical, and electronic properties of nanoscaled systems. In general, nanoscaled systems fall into two categories: those having nanostructures with positive curvature and those having nanostructures with negative curvature. In comparison with nanostructures with positive curvature, the nanostructures with negative curvature (e.g., nanocavities, nanotubes, groove nanostructures, hollow nanospheres, and shell−core configurations, etc.) have attracted much more attention because of their unique applications in mesoscopic physics and the fabrication of nanoscaled devices, which not only provide one kind of good model system to study electrical and thermal transport in nanosized confines but are also expected to play an important role as both connectors and functional units in fabricating electronic, optoelectronic, and magnetic storage devices with nanoscaled dimension.[1−8] For example, nucleation inside groove structures and nanotubes with negative curvature is favored by the Gibbs free energy, as is demonstrated by extensive experiments and calculations.[9,10] The additional work induced by the negative curvature in nanotubes should be considered based on the Laplace−Young equation. Moreover, in contrast to nanostructures with positive curvature, the nanostructures with negative curvature have the inverse physical and chemical properties such as in functionalities of the densified charge, the single bond energy, the surface stress or surface free energy, etc.[11−16] So far, many attempts have been made to investigate nanostructures with negative curvatures experimentally, using thermal treatment, the coordination polymer approach, the Kirkendall effect, and so on.[17−19] Meanwhile, many novel phenomena requiring new theoretical explanations have been seen during these experiments.

As we know, the surface and interface energies are the most important physical attributes of nanostructures because the ratio of surface-to-volume will increase with decreasing

10.1021/cr900055f CCC: $71.50
Published on Web 08/11/2009

Gang Ouyang (G. Ouyang) received his Ph.D in Condensed Matter Physics under the supervision of Professor G. W. Yang from the Zhongshan (Sun Yat-Sen) University of China in 2007. He held a research fellow position at Nanyang Technological University in Singapore before joining the physics faculty at Hunan Normal University of China in 2009, where he is currently a full professor in Condensed Matter Physics. His research interests include thermodynamic theory as applied to small systems, theoretical prediction of the physical and chemical properties of nanostructures, and multicomponent interactions in low-dimensional growth.

Chengxin Wang (C. X. Wang) received his Ph.D in Condensed Matter Physics from Jilin University of China in 2002. He held a postdoctoral position at Zhongshan (Sun Yat-sen) University of China in 2003 and a JSPS postdoctoral researcher position at the Tokyo Institute of Technology of Japan in 2005 before joining the materials science faculty at Zhongshan (Sun Yat-sen) University of China in 2007, where he is currently a full professor in Materials Physics and Chemistry. His research interests include the thermodynamic nucleation and growth kinetics of metastable phases at the nanometer scale, diamond and related materials, and semiconductor nanomaterials and nanostructures.

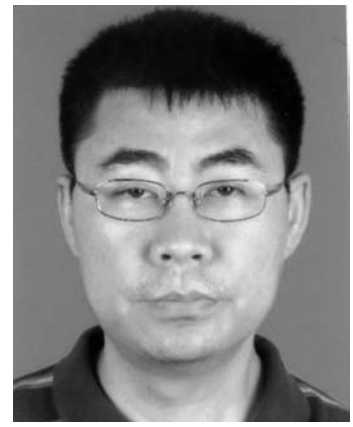

Guowei Yang (G. W. Yang) received his Ph.D in Materials Physics and Chemistry at Tsinghua University of China in 2000. He held a postdoctoral position at the University of Illinois at Urbana−Champaign of the United States of America before joining the materials science faculty at Zhongshan (Sun Yat-sen) University of China in 2002, where he is currently a full professor of Materials Physics and Chemistry. His research interests include the thermodynamic nucleation and growth kinetics of metastable phases at the nanometer scale, synthesis of nanocrystals and nanostructures with metastable structures and shapes under moderate, not extreme, conditions, and the surface and interface of nanomaterials.

size. Therefore, surface and interface energies will greatly affect the physical properties of nanostructures. Importantly, the anomalous surface energy of nanostructures always induces many novel nanosized-effects, which open many windows on technological potentials. However, there is a fundamental issue here in that there has not been a clear and detailed understanding of the surface energy of nanostructures with negative curvature in the reported physical and chemical investigations of them. In other words, we do not have a clear and general insight into the basic physics and chemistry involved in the surface energy of nanostructures with negative curvature. Therefore, it is essential to develop new theoretical tools for the understanding and determination of the surface energy of nanostructures with negative curvature.

In this review, we will survey for this issue the status and progress so far of the established thermodynamic approaches to the nanoscale for elucidating and calculating the surface energy of nanostructures with negative curvature. First, we introduce the fundamental concepts and methods of the proposed thermodynamic approaches to the nanoscale, including our own investigations for the surface energy of nanostructures with negative curvature. Second, taking typical nanostructures with negative curvature such as nanocavities, nanotubes, and nanopores as examples, we summarize the application of the theoretical tools developed to address surface energy and related size effects. Importantly, the thermodynamic approaches on the nanoscale for the surface energy of nanostructures with negative curvature not only reveal the new physics and chemistry involved in the surface energy at the nanometer scale but also provide general theoretical tools to calculate the surface energy. Therefore, we expect these thermodynamic models to be general methods for understanding the surface energy of nanostructures with negative curvature.

This review is organized as follows. First, in sections 1 and 2, we introduce the fundamental outlines of the thermodynamics of nanomaterials based on the liquid drop models, the bond relaxation approach, and Hill's theory. Second, in section 3, we present a universal analytical model both from the perspective of thermodynamics and of continuum medium mechanics to elucidate the surface energy of nanocavities and their relevant novel physical and chemical properties. Third, in section 4, the surface energy of nanotubes at their inner skin and outer surface and their mechanical behaviors are clarified. Finally, in section 5, we consider the size effects of alloy formation in the shell−core nanostructures from both the thermodynamic and diffusion kinetic viewpoint. Additionally, the conclusions to be drawn from this review are summarized in section 6.

2. Surface Energy of Nanostructures with Negative Curvature

2.1. Overview

In general, the physical and chemical properties of a macroscopic system can be well-characterized by classical

thermodynamics or continuum medium mechanics, which relate measurable quantities directly to applied stimuli such as pressure, temperature, and external fields. In addition, quantum effects are key factors for systems at the atomic scale, and physical and chemical quantities can be evaluated by solving the relevant Schödinger equations. Nevertheless, for systems at the nanometer scale, both classical methods and quantum approaches involve some difficulties. For low-dimensional systems, edge state, end state, surface or interface tapping, and broken bonds need to be taken into account. Finding effective ways to deal with these difficulties has been a long-standing challenge.

Consequently, thermodynamics at the nanoscale is becoming an increasingly relevant method as the dimension of electronic devices approaches the nanoscale. The coordination deficiency and atomic bond contraction at the surface or the interface layer makes nanoscaled systems differ in properties from their corresponding bulk counterparts. For example, Au−Au bond contraction will take place in the outermost two atomic layers of nanomultilayers, as is confirmed by electron cohesive diffraction.[20] The mean lattice constant of Co nanoislands deposited on Cu contracts by 6% compared with the bulk value, as is verified by theoretical calculations and scanning tunneling microscopy measurements.[21] In other words, the surface or interface phase plays a significant role with decreasing size. Accordingly, the surface or interface energy is an important physical quantity for nanoscaled systems.

Thermodynamically, the surface energy γ is defined as the reversible work per unit area involved in creating a new surface at constant temperature, volume, and total number of moles. We should point out that the three terms "surface energy", "surface stress", and "surface tension" have been frequently confused. In general, the relationship of the surface energy and the surface stress tensor is $g_{\alpha\beta} = A_0^{-1}\,\partial(\gamma A_0)/\partial\varepsilon_{\alpha\beta}$ ($\alpha,\beta = 1,2$), in which A_0 and $\varepsilon_{\alpha\beta}$, respectively, are the surface area per atom and the strain tensor.[22] For a liquid, the diagonal components of $g_{\alpha\beta}$ are numerically equal to γ. However, the $g_{\alpha\beta}$ is not equivalent to γ for a solid. The energy γ is required to create unit area of surface. Fischer and co-workers clarified the definitions for surface energy, surface tension, and surface stress in some detail in a recent review.[23]

It is well-known that many physical quantities such as melting point, surface energy, interaction energy, and bond length show size effects when specimens approach the nanoscale.[24−26] For instance, the typical nanostructures with the negative curvature, i.e., the surface-segregated nanoparticles with shell−core configurations, are produced in the Pd−Ag alloying system, the components of which are miscible in the bulk phase.[27] Also, a series of shell−core bimetallic nanoparticles such as Au−Ag,[28−30] Au−Pt,[31] and Ag−Pd[32] systems were produced by a variety of chemical methods. Interestingly, Meisei and co-workers[28] demonstrated the anomalous size dependence of spontaneous interfacial alloying in shell−core nanostructures at ambient temperatures, thus indicating that size effects are apparent in these binary metallic systems. Likewise, the elastic vibrational modes in shell−core nanoparticles show controllable behaviors dependent on overall size and shell thickness, as is confirmed by Brillouin light-scattering measurments and numerical calculations.[33]

On the other hand, nanostructures with negative curvature, such as porous materials with small holes, have a prodigious combined surface area and can enhance chemical reactions and yield high-value products.[34−37] These nanostructures can allow only single molecules or clusters of certain shapes and sizes to move through the pores.[38] In a recent letter, Lee and colleagues[39] reported that, at room temperature, with no change in electrical transport properties, the thermal conductivity of n-type crystalline Si with periodically arranged nanometer-sized pores may be lowered by up to 2−4 orders of magnitude from that of bulk silicon, depending on the size and spacing of the pores. Importantly, this exciting result indicates that nanoporous semiconductors with aligned pores may be highly attractive materials comparable to those currently used for thermoelectric applications but much easier to manipulate. Further, as found by Zhu et al., nanocavities in the host matrix show instabilities during electron beam irradiation.[40] More interestingly, the shrinkage behavior shows a unique nonlinear character with the cavity radius size contracting to about 4 nm. Moreover, the shrinkage rate becomes slower as the cavity size decreases, and finally no detectable size change is observed after the cavity size is about 2 nm.[40] In addition, the atomic vacancies or point defects with imperfect coordination numbers for nearby atoms would have a large influence on the mechanical strength of a material. It is generally known that vacancies can act as pinning centers, restraining the motion of dislocations and thus enhancing mechanical strength. For example, Smmalkorpi et al. studied the mechanical strength of carbon nanotubes with vacancies and related defects by analytic continuum theory and found that atomic defects played a dominant role in determining mechanical properties.[41] Also, carbon nanotubes are much stiffer than bulk graphite,[42,43] with Young's modulus increasing as the wall thickness is reduced.[44]

Indeed, new opportunities for using negative curvature have led to dramatic changes in many physical and chemical properties that are conventionally understandable in comparison with bulk specimens and nanostructures with positive curvature. The examples of the surface and size effects of negative curvature on various properties are endless, as has been reviewed and developed by many researchers.[40,45] The surface effects on related chemical and physical properties from the introduction of nanostructures with negative curvature has inspired a number of theoretical models and experimental observations, all of which are discussed from various aspects.

2.2. Fundamental Aspects

2.2.1. Classical Approach

Considering a single-phase system with surface or interface phase in a thermodynamic equilibrium state, the internal energy U is

$$U = TS - pV + \mu N + \gamma A \qquad (2\text{-}1)$$

where T, S, p, V, μ, N, and A are, respectively, temperature, entropy, pressure, volume, chemical potential, number of particles, and area. The differentials of the internal energy of the entire system and of other thermodynamic quantities can be deduced to be

$$\mathrm{d}U = T\mathrm{d}S - p\,\mathrm{d}V + \mu\,\mathrm{d}N + \gamma\,\mathrm{d}A \qquad (2\text{-}2)$$

$$dF = -SdT - pdV + \mu dN + \gamma dA \quad (2\text{-}3)$$

$$dG = -SdT + Vdp + \mu dN + \gamma dA \quad (2\text{-}4)$$

$$dH = TdS + Vdp + \mu dN + \gamma dA \quad (2\text{-}5)$$

$$d\Omega = -SdT - pdV - Nd\mu + \gamma dA \quad (2\text{-}6)$$

where F, G, H, and Ω denote the Helmholtz free energy, Gibbs free energy, enthalpy, and grand canonical potential, respectively. Thus, in terms of above equations, the surface tension can be defined as

$$\gamma = \left(\frac{\partial U}{\partial A}\right)_{S,V,N} = \left(\frac{\partial F}{\partial A}\right)_{T,V,N} = \left(\frac{\partial G}{\partial A}\right)_{T,p,N} = \left(\frac{\partial H}{\partial A}\right)_{S,p,N} = \left(\frac{\partial \Omega}{\partial A}\right)_{T,V,\mu} \quad (2\text{-}7)$$

From the above, we see that the surface tension is the Gibbs free energy per unit area at constant temperature, pressure, and number of particles, and also that it can be expressed as other thermodynamic functions in terms of internal energy, Helmholtz free energy, enthalpy, and the grand canonical potential, respectively. Furthermore, the surface entropy, surface enthalpy, and the coefficient of surface energy can be deduced based on the above equations:

$$s^s = -\frac{\partial \gamma}{\partial T} \quad (2\text{-}8)$$

$$h^s = \gamma + Ts = \gamma - T\frac{\partial \gamma}{\partial T} \quad (2\text{-}9)$$

$$u^s = \gamma - T\frac{\partial \gamma}{\partial T} - p\frac{\partial \gamma}{\partial p} \quad (2\text{-}10)$$

It should be noted that the relations $(\partial\gamma)/(\partial T) < 0$ and $(\partial\gamma)/(\partial p) > 0$ hold.[46] The surface energy can be calculated conventionally by semiempirical methods based on a broken bond rule,[47] i.e., the surface energy is determined by the number of bonds that have to be broken in order to create a unit area of surface. The relation is specified by

$$\gamma_{hkl} = \frac{W_{hkl}}{2A_{hkl}} \quad (2\text{-}11)$$

where W is the reversible work involved in creating a new surface. The subscripts h, k, and l represent the Miller indices specifying the orientation of a plane. Therefore, the surface energy is equivalent to the total binding energy of the surface atoms.

$$\gamma_{hkl} = \frac{n_{hkl}E_b}{2} \quad (2\text{-}12)$$

where n_{hkl} and E_b are the number of broken bonds and the binding energy of a pair of atoms, respectively. On the other hand, the interface is defined as the transition region between two joined phases. Therefore, the internal energy of the interface phase can be obtained by

$$dU^I = TdS^I + \sum_i \mu_i dn_i^I + \gamma^I dA \quad (2\text{-}13)$$

The superscript I denotes the interface phase. Since the Helmholtz free energy in the equilibrium state is $F^I = U^I - TS^I$, the interface energy takes the form

$$\gamma^I = \left(\frac{\partial F^I}{\partial A}\right)_{T,n_i^I} \quad (2\text{-}14)$$

2.2.2. Nanothermodynamics

As the dimension of a system becomes small, some questions may emerge. The conventional theoretical methods, including classical thermodynamics and quantum theory, are not suitable for addressing the novel physical and chemical properties (mechanical, thermal, acoustic, optical, electronic, and magnetic, etc.) of low-dimensional systems. Many properties of nanosolids, such as their melting point and Young's modulus, no longer remain constant with size and can indeed be tuned with the size. Many approaches have been developed for exploring this fascinating field. For example, in terms of the liquid drop model, the total cohesive energy (E_c) of nanoparticles containing N atoms is given by

$$E_c = a_v N - 4\pi r_a^2 N^{2/3}\gamma \quad (2\text{-}15)$$

with

$$a_{v,R} = a_v - 3v_0\gamma/r \quad (2\text{-}16)$$

where v_0, r_a, r, $a_{v,R}$, and a_v denote the atomic volume, the radius of an atom with sphere shape, the radius of the nanoparticles, the cohesive energy per atom and the bulk,[48−50] respectively. Further, it has also been shown by Rose et al.[51,52] that there exists a general relationship between the cohesive energy per atom and the surface energy, to wit,

$$a_{v,R} = a_v - a_s(r_0/r) \quad (2\text{-}17)$$

where $a_s = 4\pi r_a^2\gamma$. More surprisingly, the mean slope of 5.75 corresponding to eq 2-17 can be obtained for fcc and bcc crystals based on the effective coordination method,[53] which is valid for most materials.[54] So, most of the other physical quantities, such as melting temperature, Debye temperature, heat capacity, etc., are related to the size-dependent cohesive energy.

It is easily seen that, in low-dimensional systems, the surface effect plays a significant role in determining the binding energy per atom. In fact, a size effect is observed for many other physical and chemical properties. For example, the bond length between atoms which are not fully coordinated contracts spontaneously in the top three atomic layers of nanostructured materials.[55] Furthermore, the solid solubility limit in nanometer-sized binary alloying systems, the interaction binding energy, the melting enthalpy, and the melting entropy, etc., are all size-dependent.[26,56] Therefore, the above equations are no longer applicable in small systems. Also, surface effects, edge effects, system rotation and translation, etc., all influence the properties of small systems.

In addition, the recently developed bond-order-length-strength (BOLS) correlation mechanism is suitable for coping with the unusual behavior of low-dimensional systems.[57] It follows from the considerations of Goldschmidt,[58] Pauling,[59] and Feibelman,[60] that the bond will shorten spontaneously due to coordination number imperfections and the associated bond energy will increase compared with the ideal case of the bulk. Thus, the shortened and strengthened bonds and the depression of the pair potential are the physical origins

of the anomalous tunable properties of low-dimensional systems. From the fundamental perspective of the BOLS correlation mechanism, the mean relative change of a measurable quantity (Q) of a nanosolid involving N_j atoms can be written as[61]

$$\frac{\Delta Q(K_j)}{Q(\infty)} = \sum_{i\leq 3} \gamma_{ij} \frac{\Delta q_i(z_i, E_i, d_i)}{q(z, E_b, d)}$$
$$\gamma_{ij} = \frac{\Delta V_i}{V_j} \approx \frac{\tau\, c_i}{K_j} \leq 1 \qquad (2\text{-}18)$$
$$K_j = R_j/d_0$$

with

$$Q(\infty) = N_j q_0 \qquad (2\text{-}19)$$

where K_j is the dimensionless form of the solid size, which is the number of atoms aligned along the radius of a spherical dot or a rod, or across the thickness of a thin plate. R_j and d_0 denote the radius of the nanosolid and the size of an atom, respectively. τ is the dimensionality of a thin plate ($\tau = 1$), a rod ($\tau = 2$), and a spherical dot ($\tau = 3$). q_0 and q_i correspond to the local density of Q inside the bulk and the ith atomic layer. γ_{ij} is the volume ratio of a certain atomic layer, denoted i. c_i is the coordination number dependence of the bond-contraction coefficient. The bond length d will shift to d_i, where $d_i = c_i d$, and bond strength will change from E_b to E_i according to $E_i = E_i^{-m} E_b$, and hence will affect the localization and densification of charge proportionally to E_i/d_i^3. Consequently, bond strain and bond strength gains induced by broken bonds or quantum trapping cause localization and densification of the energy, which leads to excessive energy storage in the surface skin or at sites surrounding atomic defects, which not only affects the directly related properties but also perturbs the Hamiltonian and related effects such as band gap expansion, Raman phonon stiffening or softening, core level shift, and enhancement of the electroaffinity (i.e., separation between the vacuum level and the conduction band edge). Importantly, the surface strain induced by broken bonds extends only to several atomic layers, as is confirmed by the size-dependent surface free energy and related physical and chemical properties of nanocrystals, nanowires, and nanocavities.[12,62,63]

Most strikingly, the thermodynamics of small systems at the equilibrium state, developed in the pioneering work of Hill in the early 1960s,[64−68] is an effective tool to deal with mesoscopic systems. A series of recent publications by Hill et al. addressed this interesting subject in detail.[69−74]

Hill generalized the classical approach by considering the ensemble level rather than the single-system level. The core idea is the "*subdivision potential*" proposed based on classical thermodynamics. Thus, the internal energy is described in the form

$$\mathrm{d}U_t = T\mathrm{d}S_t - p\mathrm{d}V_t + \sum_i \mu_i \mathrm{d}N_{it} + \Xi \mathrm{d}\xi \qquad (2\text{-}20)$$

where t is the whole ensemble of small systems. $\Xi = (\partial U_t/\partial\xi)_{S_t,V_t,N_{it}}$. Ξ is a kind of system chemical potential being defined as the "*subdivision potential*". It is noted that the term $\Xi\ \mathrm{d}\xi$ in the above equation does not contribute appreciably to macroscopic systems, which have $\Xi = 0$. Ξ may be regarded as a function of T, p, and μ_i with intensive properties at the ensemble level.

Integrating the above equation from $\xi = 0$ to ξ and holding all small-system properties constant, we obtain

$$U_t = TS_t - pV_t + \sum_i \mu_i N_{it} + \Xi\xi \qquad (2\text{-}21)$$

For a single small system,

$$U = TS - pV + \sum_i \mu_i N_i + \Xi \qquad (2\text{-}22)$$

or

$$\Xi = U - TS + pV - \sum_i \mu_i N_i \qquad (2\text{-}23)$$

The Ξ is a new feature of nanothermodynamics. Furthermore, differentiating in the above equation, we can obtain

$$\mathrm{d}\Xi = -S\mathrm{d}T + V\mathrm{d}p - \sum_i N_i \mathrm{d}\mu_i \qquad (2\text{-}24)$$

In fact, the left-hand side is zero in macroscopic thermodynamics. In addition, the right-hand side is zero, showing the Gibbs−Duhem relation. On the other hand, the relations among S, V, N_i, T, p, μ, and subdivision potential Ξ are seen to be

$$-S = \left(\frac{\partial \Xi}{\partial T}\right)_{p,\mu_i} \qquad (2\text{-}25)$$

$$V = \left(\frac{\partial \Xi}{\partial p}\right)_{T,\mu_i} \qquad (2\text{-}26)$$

$$N_i = \left(\frac{\partial \Xi}{\partial \mu_i}\right)_{T,p,\mu_j} \qquad (2\text{-}27)$$

Furthermore, it is worth noting that Chamberlin et al.[75−84] have developed Hill's theory by considering independent thermal fluctuations inside bulk materials. On the basis of Hill's considerations, they obtained the mesoscopic mean field model, which can provide a common physical basis for many empirical properties such as magnetism, phase transitions, etc. In the following section, taking the nanocavity as an example, we will present a universal analytical method from the perspective of the nanothermodynamics and the continuum medium mechanics to elucidate the surface energy of nanostructures with the negative curvature cavities and highlight the relevant physical and chemical properties induced by the size-dependent surface energy.

3. Surface Energy of Nanocavity

3.1. Background

Nanocavities, as a sort of typical nanostructure with negative curvature, are defined as a cluster of many vacancies in a given matrix, like inverse opals, and have attracted much interest in recent years because of their potential applications in mesoscopic physics, biology, medicine, and electronic nanodevices processing, for example.[85−88] Nanocavities have been produced experimentally in Si,[89−91] Ni,[92] amorphous Ge,[93,94] and Al[95] by ion irradiation followed by thermal annealing in inert gases. The striking difference between nanocrystals and nanocavities is that the latter possess

negative curvature. The dangling bonds at the negatively curved surface could provide a large driving force for instabilities. Interestingly, there are some abnormal physical behaviors that happen under the application of a stimulus such as thermal annealing. For instance, nanocavities in the host matrix shrink during electronic beam irradiation, and the shrinking velocity slows down as the pore size is reduced, until at 2 nm it is zero and the cavity size thereafter remains constant.[96,97] In a related experiment, the nucleation of the amorphous phase occurs near the inner skin of the cavity.[98] The surface energy of the nanocavity is important to the reported pore size shrinkage. In addition, the surface energy is of great importance in understanding the mesoscopic and microscopic processes at a surface for properties such as wettability, adhesion, diffusion, and chemical reactivity, for example, which depend on the atomic bonding state. However, the surface energy of nanocavities remains much less understood.[99] In this section, we propose an approach to elucidating the surface energy of nanocavities via an analytical solution without any freely adjustable parameters. This approach combines thermodynamics at the nanoscale and continuum mechanics,[100] to give a deeper physical insight into the surface energy of nanocavities, and has enabled us to make predictions of the shrinkage of nanocavities consistent with the experimental observations.

In fact, the surface atomic structure and interactions should be involved in surface free energy. The development of theoretical methods has already increased knowledge about the relation between surface strain and atomic bond energy states of nanostructures. For example, Dingreville and coworkers developed the incorporation of the surface free energy into continuum mechanics.[101] The results indicate that the surface free energy of nanoparticles, nanowires, and nanofilms can have a large influence on elastic behavior. The energy of atoms at the surface layer and the resulting elastic behavior differ from the bulk material. Thus, the surface atomic structure and interactions among the atoms should be accounted for in the surface free energy. According to the considerations of Fried et al.,[102] Fischer et al. established a constitutive law for the surface energy as the summation over two contributions, to wit, a mechanical part and a chemical part.[23] Importantly, these results are harmonious with our recent considerations.[12,13,100]

3.2. Thermodynamic Analytic Expression of Surface Energy

The surface energy in the inner skin of a nanocavity in a host matrix can be composed of two contributions, i.e., the chemical part (γ^{chem}) and the structural part (γ^{stru}), as in

$$\gamma = \gamma^{\text{chem}} + \gamma^{\text{stru}} \tag{3-1}$$

The chemical part of the surface energy originates from the dangling bond energy at the inner surface of the nanocavity, while the structural part is from elastic strain energy in the one atomic layer thickness of the inner skin of the nanocavity.

In terms of the relevant experiments,[97,98] we propose the model illustrated in Figure 1 for a nanocavity in a host matrix. Interestingly, the region surrounding the nanocavity will preferentially form the nonorientation order phase with atomic bond order loss.[97,98,103] Thus, we may consider the cavity matrix as two separate components, which are the liquid-like β phase and the vapor-like pore α phase. Jiang et al.[104] have suggested that the surface energy difference

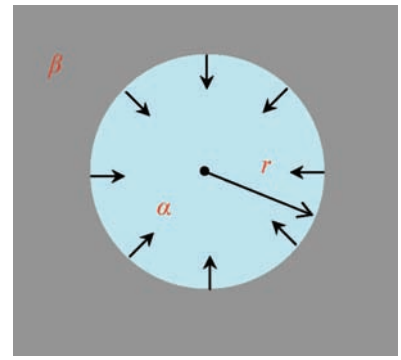

Figure 1. Schematic illustration of the two-phase structure of the vapor-like nanocavity, α, and the liquid-like matrix lattice phase, β. The arrows indicate that the nanocavity will undergo shrinkage under the larger driving force of the inner skin resulting from applied external activation. Note that the term "external activations" includes energetic electron beam irradiation, ion irradiation, and thermal annealing.

between the solid and the liquid is very small in comparison with that between the solid and the gas or between liquid and gas phases. The interface energy of liquid (l) and gas (v) or solid (s) and gas, can be approximately related as $\gamma_{\text{lv}}(D)/\gamma_{\text{lv0}} \approx \gamma_{\text{sv}}(D)/\gamma_{\text{sv0}}$, in which γ_0 is the value in the plane surface with 0 curvature, and D is the diameter of the nanosized solid. The differential of the total energy in the system should follow the relation

$$\begin{aligned} \mathrm{d}E &= \mathrm{d}E^{\alpha} + \mathrm{d}E^{\beta} + \mathrm{d}E^{\mathrm{S}} \\ &= T\mathrm{d}S^{\alpha} - p^{\alpha}\mathrm{d}V^{\alpha} + \mu^{\alpha}\mathrm{d}N^{\alpha} + T\mathrm{d}S^{\beta} - p^{\beta}\mathrm{d}V^{\beta} + \\ &\quad \mu^{\beta}\mathrm{d}N^{\beta} + T\mathrm{d}S^{\mathrm{S}} + \mu^{\mathrm{S}}\mathrm{d}N^{\mathrm{S}} + \gamma^{\text{chem}}\mathrm{d}s - C\mathrm{d}c \end{aligned} \tag{3-2}$$

where E, S, V, N, and T represent the energy, entropy, volume, number of moles in the system, and absolute temperature; and C, μ, s, and c are the curvature term with an external force as defined by Gibbs, the chemical potential, the interfacial area, and the curvature, respectively.[105] The N^{S} is the actual excess in moles over the amount computed, which supports the dividing surface between the α phase and β phases. Since the volume of the surface phase is negligible, so is N^{S}. The superscripts α, β, and S denote quantities relating to the pair of phase regions, α and β, and surface phase S. We note the relations

$$\begin{aligned} V &= V^{\alpha} + V^{\beta} \\ E &= E^{\alpha} + E^{\beta} + E^{\mathrm{S}} \\ S &= S^{\alpha} + S^{\beta} + S^{\mathrm{S}} \\ N &= N^{\alpha} + N^{\beta} + N^{\mathrm{S}} \end{aligned} \tag{3-3}$$

At equilibrium the chemical potentials will be identical, i.e., $\mu = \mu^{\alpha} = \mu^{\beta} = \mu^{\mathrm{S}}$, so considering the above relations we obtain

$$\mathrm{d}E = T\mathrm{d}S - p^{\alpha}\mathrm{d}V^{\alpha} + \mu\,\mathrm{d}N - p^{\beta}\mathrm{d}V^{\beta} + \gamma^{\text{chem}}\mathrm{d}s - C\mathrm{d}c \tag{3-4}$$

A differentiation of the integration of the equation at constant curvature leads to the curvature-dependent surface energy

$$(\partial\gamma^{\text{chem}}/\partial c)_{\mathrm{T}} = -C/s \tag{3-5}$$

Comparing with the Tolman[106] and Koenig[107] formula based on the surface tension $((\partial\gamma^{chem})/(\partial c))_T = [-2\delta\gamma^{chem}(1 + \delta c + (\delta c)^2/3)]/[1 + 2\delta c(1 + \delta c + (\delta c)^2/3)]$ and replacing the curvature c with $-r^{-1}$, we obtain

$$\left(\frac{\partial\,\gamma^{chem}}{\partial\,r}\right)_T = \frac{\gamma^{chem}}{r}\frac{1}{\dfrac{r}{2\delta\left(1 - \dfrac{\delta}{r} + \left(\dfrac{\delta}{r}\right)^2/3\right)} - 1} \quad (3\text{-}6)$$

where δ is the Tolman's length. With the inner wall thickness given by h, in the special case of a spherical cavity of diameter $d = 2r$, eq 3-7 yields

$$\frac{\gamma^{chem}_{sv}(d)}{\gamma^{chem}_{sv0}} \approx \frac{\gamma^{chem}_{lv}(d)}{\gamma^{chem}_{lv0}} = 1 + \frac{4h}{d} \quad (3\text{-}7)$$

Importantly, the difference between eq 3-7 and the similar relation proposed by Kirkwood and Buff[108−110] is the positive sign.

Similarly, for γ^{stru}, the density of surface strain energy in eq 2-26, Saito et al. investigated a two-dimensional crystal with a square lattice and obtained the total elastic stain energy of the rigid structure.[111] The results indicate that the elastic strain in the surface unit cell plays a vital role in determining the total energy. The spontaneous stress situation arises from defects such as adsorbed atoms or from steps and reaches the energy minimum. In our case, we treat the spherical face of a nanocavity in a host matrix and furthermore consider the reconstruction and relaxation of the surface. The elastic strain energy induced by the negative curvature is involved in the surface energy in the inner skin of nanocavities. According to the Laplace−Young equation,[112] the pressure difference (Δp) between the interior and exterior of the spherical nanocavity can be expressed in terms of the inner surface diameter (d) of the cavity as

$$\Delta p = -4f/d \quad (3\text{-}8)$$

where f is the surface stress. The compressibility κ and strain ε of the matrix are given by $\kappa = -\Delta V/(V\Delta p) = \Delta V d/2fV$ and $\varepsilon = \Delta a^*/a^* = \Delta A/(2A) = \Delta V/(3V)$, respectively, where V, A, and a^* represent the volume, the surface area of the spheric nanocavity, and the distance between two near-neighbor atoms. The latter distance is taken to be approximately equal to the lattice constant of the crystalline phase in our case. Thus, we have $\varepsilon = (\Delta a^*)/(a^*) = (2k)/(3d)\sqrt{(d_0 h S_{mb} H_{mb})/(kV_s R)}$,[113,114] in which d_0, h, S_{mb}, H_{mb}, V_s, and R denote the critical value of the void,[115] the atomic diameter, the melting entropy, the melting enthalpy, the molar volume, and the ideal gas constant, respectively. Similarly, the surface strain ($\varepsilon^s_{\alpha\beta}$) of a sphere is related to the bulk strain (ε_{ij}) within the particle through a coordinate transformation as $\varepsilon^s_{\alpha\beta} = t_{\alpha i} t_{\beta j} \varepsilon_{ij}$, where α, β range from 1 to 2, i, j range from 1 to 3, and $t_{\alpha i}$ is the transformation tensor. Therefore, from the above relations, the structural part of surface energy can be obtained as

$$\gamma^{stru} = \varepsilon^2 \bar{\alpha} \quad (3\text{-}9)$$

where $\bar{\alpha}$ is the spring constant averaged over pairs of atoms in the deformation lattice of the inner cavity wall.

3.3. Size Effects Induced by Surface Energy

In this section, we use the spherical coordinates (r, θ, ϕ) relative to the center of the spherical cavity. The deformation behavior of the inner wall in the matrix can be derived based on the theory of linear elasticity. As for the special case of spherical symmetry, the values of the strain components, stress components, and displacements are dependent on the radial coordinate r and are independent of θ and ϕ. The equilibrium equation and volume strain ε are written as

$$\frac{\partial\sigma_r}{\partial r} + \frac{2}{r}(\sigma_r - \sigma_T) = 0 \quad (3\text{-}10)$$

$$\varepsilon = \frac{1}{r^2}\frac{\partial}{\partial r}(r^2 u_r) \quad (3\text{-}11)$$

where σ_r and σ_T (i.e., σ_θ and σ_ϕ) are the radial and tangential stress, respectively.

In light of Hooker's law, the stress-to-strain relationships for the radial and tangential components are given by

$$\sigma_r = \lambda\,\Theta + 2\,G'\,\varepsilon_r \quad (3\text{-}12)$$

$$\sigma_T = \lambda\,\Theta + 2\,G'\,\varepsilon_T \quad (3\text{-}13)$$

, respectively, in which λ, G', and Θ are the Lamé constants and the bulk strain. Furthermore, in combination with the geometric equations (i.e., $\varepsilon_r = \partial u_r/\partial r$, $\varepsilon_T = u_r/r$), the component of the displacement u_r can be shown to be $u_r = Ar + B/r^2$, where A and B are coefficients.

Just as in the case of a nanocavity in a host matrix, the nanometer-curved surface at an atom dangling bond structure combined with a compressive stress on the inner wall of the cavity will provide a driving force for nanocavity shrinkage during external activation, as has been demonstrated by recent experiments.[97,98] The reference state of a nanocavity before shrinkage, which is in a metastable state, is produced by an initial experiment. Considering the curvature effect, we use these boundary conditions

$$\sigma_r = -(-2\gamma(a)/a + p_0) \text{ at } r = a \quad (3\text{-}14)$$

$$\sigma_r = -p_0 \text{ at } r \to \infty \quad (3\text{-}15)$$

where a and p_0 are the initial radius of the nanocavity and the normal pressure, respectively. Therefore, we can deduce that the coefficients are given by $A = (-p_0)/(3\lambda + 2G')$ and $B = -(a^2\gamma(a))/(2G')$. Furthermore, the u_r can be calculated as shown in eq 3-16:3-16

$$u_r = -rp_0/(3\lambda + 2G') - a^2\,\gamma(a)/(2\,G'r^2) \quad (3\text{-}16)$$

with $\lambda = E\nu/[(1 + \nu)(1 - 2\nu)]$ and $G' = E/[2(1 + \nu)]$, in which ν and E are Poisson's ratio and Young's modulus, respectively. Also, according to the definition of intrinsic bulk modulus [K] by Yang,[116] we have

$$[K] = \frac{-3(1 - \nu)}{2(1 - 2\nu)}\left(1 - \frac{2\gamma(r)}{3a\chi K}\right) \quad (3\text{-}17)$$

where χ and K are the magnitude of the maximum strain and the bulk modulus of the elastic matrix, respectively.

Herein, we analyze the inner surface characteristics during the process of nanocavity shrinkage. Taking a nanocavity in the silicon matrix as an example, we calculate the chemical

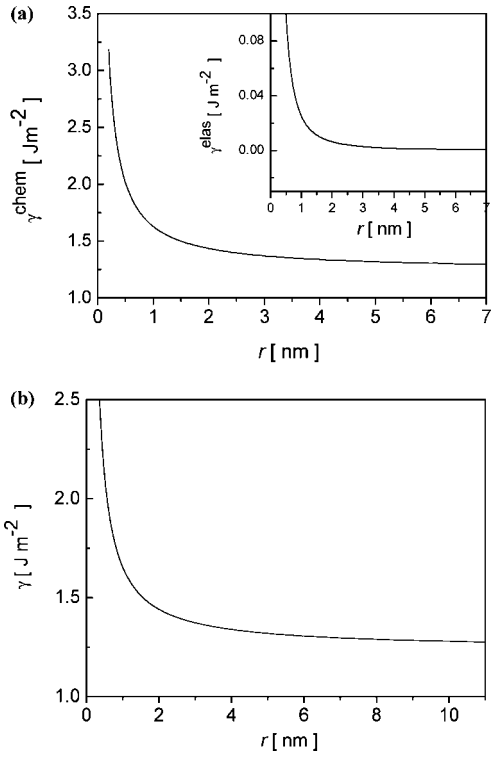

Figure 2. Size-dependent inner surface elastic energy (the inset) and chemical energy with (a) total surface free energy with (b) for Si.

energy, the elastic strain energy, and the total surface energy as shown in Figure 2. It is shown that both the chemical energy and the elastic strain energy of the nanocavity increase with reduction of cavity size. Figure 2b shows that the total surface energy of the nanocavity increases when the cavity size is reduced.

From the perspective of nanocavity surface energy considerations, we can find that a size of 2 nm seems to be a threshold value for the *size dependence* of nanocavities in a Si matrix, as is shown in Figure 2. In other words, a radius of 2 nm seems to be the threshold at which the surface energy becomes stable. Noticeably, the surface energy in nanostructures is not equivalent to the total energy of these systems since it involves bulk energy, entropy, and surface or interface terms, etc. In general, the system is stable when the total energy is equal to a minimum value. According to our calculations, the surface energy of nanocavities with a size of 2 nm is not the size at which the surface energy becomes stable, whereas it is the calculated result based on the theoretical model.

Using eq 3-16, the components of the displacement are calculated as a function of the nanocavity's radius, as shown in Figure 3a. Interestingly, from Figure 3a, we can see that the theoretical predictions show the components of the displacement increasing as the size decreases. Also, the distribution of the u_r in the inner skin of a nanocavity is related to the initial size of the cavity. Note that $u_r = 400$ nm for a cavity of radius 25 nm, which is the limiting case; this means that larger displacements of components will lead to local hardening around the nanocavity because of the effect of the surface energy. Higher surface energy in the inner skin will introduce a larger stiffening zone. The curves plotted in Figure 3a depict this tendency. Furthermore, the functional dependence of u_r on a and r is shown in Figure 3b. The size dependence of the surface energy of the cavity causes the cavity to shrink and the radial component of the displacement to be less than the effect in bulk.

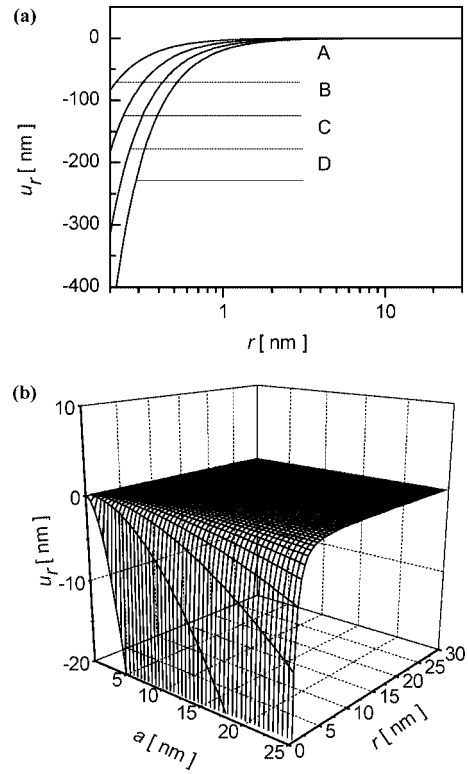

Figure 3. Distribution of the radial component of the displacement in the inner wall of nanocavity: (A) $a = 10$ nm, (B) $a = 15$ nm, (C) $a = 20$ nm, and (D) $a = 25$ nm with (a) and the a and r dependence of the radial displacement with (b).

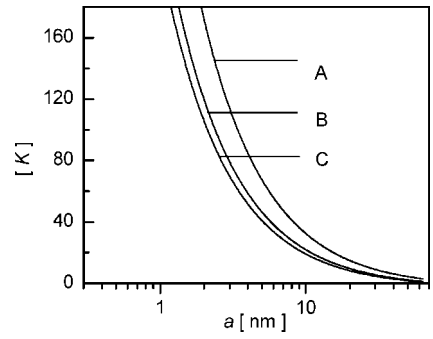

Figure 4. Size dependence of the intrinsic bulk modulus of the nanocavity in Si matrix ($\chi = 10^{-4}$): (A) $\gamma = 2$ J/m^2, (B) $\gamma = 1.4$ J/m^2, and (C) $\gamma = 1.24$ J/m^2.

Figure 4 depicts the relationships among the surface energies of the pore, matrix, and inner skin components. With increasing surface energy, the intrinsic modulus in the cavity skin becomes larger than that of the bulk. Combining the theoretical results for the components of the displacement and the intrinsic bulk modulus, we can anticipate that local hardening may take place in the cavity skin because of the surface energy size dependence. It should be indicated that the inner surface energy of a nanocavity increases monotonically for radii of about 2 nm or larger. Thus, the shrinking is faster when the cavity's radius is larger than the threshold value of 2 nm. In contrast, shrinking will be slowed for larger surface energies because of skin hardening.

3.4. Nonlinear Shrinkage

3.4.1. Observations

It is interesting to note that some physical and chemical properties would be engendered by the higher inner surface

energy of nanostructures with negative curvature as compared to zero curvature and nanostructures with positive curvatures.[63,88,117] Recently, numerous experimental[89,98,118] and theoretical[13] investigations have reported the unstable behaviors of nanocavities during external activation. For example, Zhu[40] showed experimentally that the shrinking process of nanocavities displays definitely nonlinear behavior. Bai et al.[119] reported that molecular dynamics simulations showed melting behaviors of nanocavities much different from those of the bulk trunk and nanocrystals. It is well-known that the melting temperature of nanocrystals with positive curvature is depressed with size.[57,120] However, questions may still arise concerning, for example, what will happen to a nanocavity in the matrix when the matrix starts melting? Little progress has been made in the presently available literature toward physical understanding of the melting behavior of nanocavities in a matrix.[119] In this section, we propose, based on our recent considerations, analytical kinetic and thermodynamic approaches to treating both the shrinkage of nanocavities in a matrix under external activation, and also the melting behavior when the temperature is higher than the melting point of the matrix.[12,13]

3.4.2. Kinetic Behaviors

On the basis of the considerations in section 3.2, the surface energy of a nanocavity has its thermodynamic origin in the atomic bonding energy and the elastic strain energy of the inner surface of the nanocavity.[12,13] The negative curvature of nanocavities induces a steady increase of the density of the atomic bonds with decreasing size. Similarly, the density of the elastic strain energy increases as the void size decreases. Thus, according to the theoretical results in section 3.2, the inner surface energy (γ) of a nanocavity can be attributed to two sources,[121] the chemical (γ^{chem}) and the structural (γ^{stru}), as follows

$$\gamma 5(d) = \gamma_0(1 + 4h/d) + \bar{\alpha}\varepsilon^2 \qquad (3\text{-}18)$$

where γ_0 and ε are the value of the inner surface energy in the plane surface with zero curvature and the lattice strain of the inner skin of the void, respectively. Nanocavities in the host matrix are thermodynamically metastable, which is similar to the case of the metastable nanodiamond and graphite.[10] If external activations involving irradiation and thermal annealing are applied to nanocavities, they become unstable and then shrink as observed experimentally.[122]

It is noteworthy that the crystalline structure in the nanocavity inner skin is different from the ideal bulk. Because of imperfections in the coordination numbers of atoms in the surface layer, local strain is present and is involved in the surface energy model, including the contributions from the structural and chemical sources. Also, the atomic bond lengths, strengths, and orders at the inner skin of a nanocavity are different from those of the bulk counterpart. Furthermore, as has been experimentally observed, nanocavity shapes are generally not perfect spherical voids. Therefore, the inner surface energy can be expressed as the average value of various crystalline surfaces.[123] Thus, the inner surface energy would be analytically defined by

$$\bar{\gamma} = \frac{\sum \gamma_{(ijk)} S_{(ijk)}}{\sum S_{(ijk)}} \qquad (3\text{-}19)$$

where $\gamma_{(ijk)}$ and $S_{(ijk)}$ denote the surface energy and the surface area at the (ijk) crystalline facet, respectively. Because of the amorphous matrix (short-distance order structure) around the nanocavity, we can consider the nanocavities as having a spherical shape.

On the basis of classical theory, we assume that the following conditions prevail in the shrinkage of nanocavities:

$$r|_{t=0} = r_0 \text{ and } r = r(t) \qquad (3\text{-}20)$$

Under those conditions, we further assume that the shrinkage of nanocavities is driven by the capillary force induced by the negative curvature as predicted by the Laplace−Young equation. We take into account here the possibility that, during the course of nanocavity nucleation, there may also be gas in the nanocavities. Physically, the high internal gas pressure would influence the shrinkage of nanocavities because the increase of the internal pressure counterbalances the surface tension. However, no gas remains in nanocavities at matrix temperatures above 650 °C. Under those conditions, nanocavities become nanobubbles.

Accordingly, in general, we obtain for the velocity of shrinkage of nanobubbles

$$\frac{dV}{dt} = K_{in} S_{nc}\left(\frac{2\bar{\gamma}(r)}{r} - p_{in}(r)\right) \qquad (3\text{-}21)$$

where V is the volume during the shrinkage process with $V(r) = (4)/(3)\pi(r_0^3 - r^3)$, t is the shrinking time, S_{nc} is the area of inner skin with $S_{nc}(r) = 4\pi r^2$, K_{in} is the kinetic constant with $K_{in} = K_{in0}\exp(-\Delta G_c/RT)$, and ΔG_c is the activation energy of shrinkage. $p_{in}(r)$ is the internal gas pressure, with $p_{in}(r) = p_0(r_0/r)^3$, and p_0 and r_0 are the initial gas pressure and the radius, respectively. Actually, the internal gas pressure p_0 is smaller than the value of $2\gamma(\bar{r})/r$.[124] Thus, if $p_{in}(r) = 0$, the velocity of shrinkage of nanocavities is written as

$$\frac{dV}{dt} = K_{in} S_{nc} \frac{2\bar{\gamma}(r)}{r} \qquad (3\text{-}22)$$

During shrinking, the surface energy of the inner wall of nanocavities becomes larger than that of the bulk from eq 3-18. Combining eqs 3-18 and 3-21, we obtain

$$\frac{dr}{dt} = -2K_{in}\left[\bar{\gamma}_0\left(\frac{1}{r} + \frac{2h}{r^2}\right) + \frac{\Theta}{4r^3}\right] \qquad (3\text{-}23)$$

where the factor of $\Theta = (4kd_0hS_{mb}H_{mb}\bar{\alpha})/(9V_sR)$ is called the material parameter. Thus, integrating eq 3-23, we obtain the shrinking kinetic model of nanocavities as

$$\int_{r_0}^{r} f(r)\, dr = -2K_{in}t \qquad (3\text{-}24)$$

where the function $f(r) = 1/[\bar{\gamma}_0(1/r + 2h/r^2) + \Theta/(4r^3)]$.

3.5. Phase Transition: Superheating

According to thermodynamics, the solid−liquid phase transition in a system must satisfy three criteria: mechanical, thermal, and phase equilibrium.[120] Thus, the terms in the solid−liquid phase equilibrium for a nanocavity system are given by

$$\mu^{\alpha} = \mu^{\beta} \tag{3-25}$$

$$T^{\alpha} = T^{\beta} \tag{3-26}$$

$$P^{\alpha} = P^{\beta} - \frac{2\bar{\gamma}}{r} \tag{3-27}$$

where μ and T are the chemical potential and the temperature, P is the pressure, r is the radius of the nanocavity with $d = 2r$, and the superscripts α and β denote the solid and liquid phases, respectively. Note that, in the planar case, the mechanical equilibrium condition is $P^{\alpha} = P^{\beta}$. Therefore, considering the thermodynamic relationship $d\mu = -S\,dT + V\,dP$, we have

$$S_{mb}dT = Vd\left(\frac{2\bar{\gamma}}{r}\right) \tag{3-28}$$

where $S_{mb} = S^{\beta} - S^{\alpha}$. Integrating eq 3-28, we attain the melting thermodynamic relationship of a nanocavity in the host matrix as

$$\frac{\Delta T}{T_{mb}} = \frac{4\bar{\gamma}(d)V_s}{dH_{mb}} \tag{3-29}$$

where T_{mb} is the melting temperature of bulk (matrix). Therefore, $\Delta T (= T - T_{mb}) > 0$ implies superheating of the nanocavities. Further, substituting eq 3-18 into eq 3-29, we deduce the melting model of a nanocavity in the host matrix as

$$\Delta T = \frac{4V_s\left[\bar{\gamma}_0\left(1 + \frac{4h}{d}\right) + \frac{\Theta}{d^2}\right]}{dH_{mb}}T_{mb} \tag{3-30}$$

In addition, it is noted that the initial nanocavity originates in the formation of an atomic vacancy in the lattice matrix. Generally, atomic vacancies or point defects in materials have significant effects on their physical and chemical properties such as mechanical strength and thermal stability, etc. Atomic vacancy formation energy is defined as the energy required to break all the bonds of the specific atom to its surroundings. In the 1950s, Brooks established a semiempirical model to calculate the vacancy formation energy of bulk materials with isotropic properties as $E_v = 8\pi d_0{}^3\gamma(\gamma + 2G'd_0')^{-1}$, where d_0' is the radius of the atom.[125] Furthermore, by introducing the size effect of d_0', γ, and G', the E_v of nanoparticles could be predicted.[57,126]

Combining eqs 3-23 and 3-30, we calculated the shrinking kinetics and the melting behaviors of a nanocavity in a silicon host matrix. Figure 5a shows the nonlinear shrinkage of nanocavities under electron irradiation, and the shrinking velocity (dr/dt) becomes large when the nanocavity's radius is in the range of 2−4 nm. It is reported that the shrinkage of nanocavities accounts for the cases by the ion irradiation and showed a linear dependence of nanocavity shrinkage on ion irradiation.[127,128] The shrinkage mechanism upon electron irradiation is different from that upon ion irradiation, in that the thermodynamic driving force in electron irradiation is the difference between the chemical potential of a vacancy in the matrix and a vacancy on the inner surface of the nanocavity, while the shrinkage mechanism upon ion irradiation is the external gettering of implanted atoms and the ion cascade effect. Importantly, these theoretical predictions give the same tendency for nonlinearity decrease.[40]

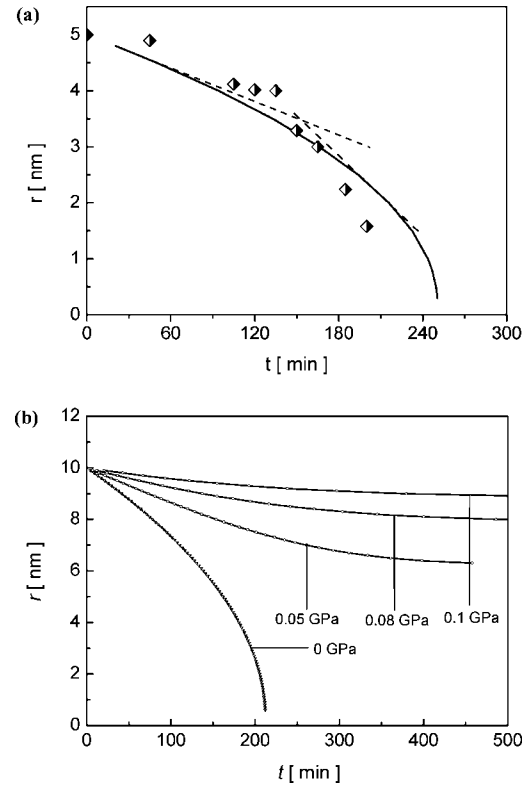

Figure 5. Nanocavity size shrinking kinetics: (a) the relationship between nanocavity size and thermal activation time. Two dashed lines mean the slopes of the curve representing different shrinking velocity, and circles are the experimental data.[40] (b) The relationship among nanobubble size, the external activation time, and the internal gas pressure.

Zhu[40] pointed out that the nanocavity stops shrinking at the critical void size of 1−2 nm, which is attributed to the local hardening around the nanocavity during the shrinking process.[13,116] The activation energy ΔG_c of shrinkage becomes large due to the formation of the hardened spherical shell and, thus, leads to K_{in} being small. According to eq 3-23, the shrinking time will become longer when the size of nanocavities becomes smaller. Thus, the smaller the size of the nanocavity, the harder is the region surrounding the inner shell of the nanocavity. As a result, the shrinking time becomes longer.

On the basis of related experiments, the rate of nanocavity shrinkage is evidently enhanced in the amorphous phase.[129] In fact, the activation energy of shrinkage in a crystalline phase is larger than that in an amorphous phase.[130,131] This large activation energy can lead to the small kinetic factor K_{in} and the long shrinkage time. Thus, the shrinkage velocity in the amorphous phase is faster than in the crystalline phase. On the other hand, the influence of the internal gas pressure on the shrinkage of nanobubbles under an external activation is as shown in Figure 5b. Clearly, the internal gas pressure can effectively slow down the shrinking velocity with decreasing nanobubble size. Accordingly, the shrinkage of nanocavities is a process involving competition among the capillary force induced by the negative curvature, the local hardening induced by the surface energy, and the internal gas pressure.

Figure 6 shows the dependence on nanocavity size of matrix nanocavity melting temperatures based on eq 3-30. When $d < 5$ nm, the superheating temperature of nanocavities

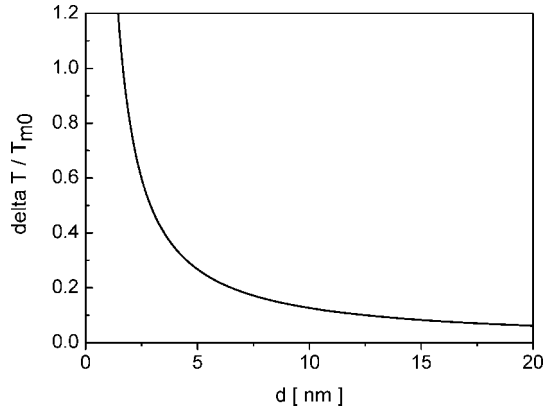

Figure 6. Size dependence of the melting temperature of nanocavities.

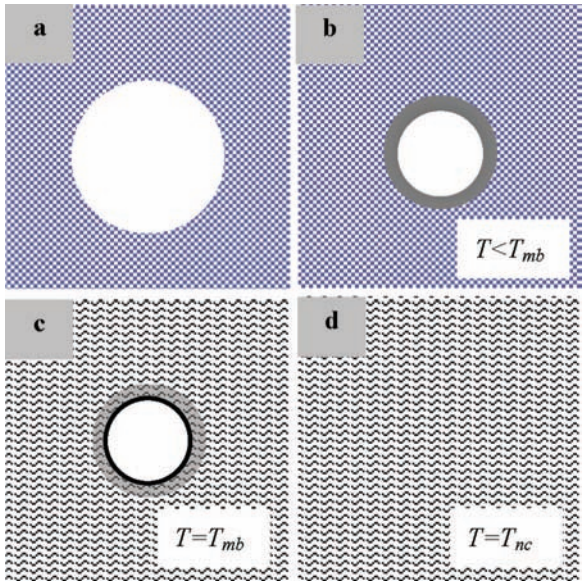

Figure 7. Schematic illustration of a complete size shrinking and melting process of nanocavities in a matrix. (a) A nanocavity in the host matrix starts to shrink (b) when it is annealed associated with local stiffening around the inner skin. (c) Matrix melts first, and then the skin stiffens. (d) Nanocavities vanish when the temperature is raised further.

rapidly increases with decreasing size. However, when $d >$ 5 nm, nanocavities show only weak superheating, and finally the melting temperature of the nanocavities and the host matrix becomes identical ($\Delta T = 0$).

Interestingly, these theoretical results are quite consistent with molecular dynamics simulations.[119] Thus, we have a complete picture of the melting of a nanocavity in a host matrix as shown in Figure 7. In detail, a nanocavity in the host matrix shrinks when an external thermal activation is applied. The kinetics of shrinkage displays nonlinear character, and local hardening forms around the inner skin of the nanocavity because of the size effect of the nanocavity inner surface energy (Figure 6). Meanwhile, the shrinkage of the nanocavity stops when its size is close to a critical value below which the nanocavity is thermodynamically stable, and its size does not change under thermal annealing. First, when the temperature is raised to the matrix melting point ($T = T_{mb}$), the matrix melts, becoming liquid, but nanocavities are still stiffening in the melting matrix because of the superheating effect (Figure 7c). Then, when the temperature is raised to the nanocavity melting temperature ($T = T_{nc}$), the nanocavities collapse, and the host matrix finally becomes homogeneous.

The melting behavior of a nanocavity has different characteristics than the melting behavior of a free nanocrystal.[120] Free nanocrystals have positive curvature, and their melting temperatures are usually below that of the corresponding bulk due to the size-dependent surface energy.[26] However, nanocavities have negative curvature in the matrix and exhibit superheating as discussed above. The size effect of the inner surface energy of nanocavities induced by the negative curvature seems to be the physical origin of the unusual melting behaviors.

3.6. Sink Effect

3.6.1. Observations

It is generally known that metal contaminants such as Au, Ag, and Cu in silicon-based micro/nanointegrated circuits form the centers of deep levels that dramatically depress the minority carrier lifetime thus reducing device performance.[88,132] Interestingly, it has been experimentally confirmed that metallic impurity atoms sre efficiently trapped near nanocavities in a silicon host matrix.[117,133−138] Moreover, artificial cells with nanocavities can sequester poisonous heavy elements such as heavy metal atoms in the human body.[96] The void volume and inner skin associated with such nanocavities are the preferred trapping centers for impurities.[124,139,140] Thus, it is important to note that gettering by nanostructures with negative curvature is an important aspect for potential applications of micro/nanodevices. For example, some impurities such as metallic contamination need to be gettered in semiconductor devices. Experimentally, many impurities in semiconductor devices, including Fe, Co, Pd, Ag, and others, have been gettered by nanocavity structures.[132,135,141,142]

However, this raises the question of why nanocavities in host crystals can trap metallic impurity atoms. The answer to this fundamental question is not clear so far.[13] In general, the physical properties of nanocavities are greatly different from those of nanocrystals because of the negative curvature of the inner surface of nanocavities.[143] Thus, we propose in this section that, for metallic impurity atoms, the sink effect of nanocavities in a host crystal be based on the established thermodynamic and kinetic approach.[10] Our theoretical results not only reveal the physical mechanism for the trapping of metallic impurity atoms by nanocavities in a host crystal but also result in theoretical predictions that are consistent with experiments.

3.6.2. Nucleation Thermodynamics in Nanocavities

First of all, we constructed the schematic illustration of a spherical nanocavity in the host matrix as shown in Figure 8. In the light of related experimental observations, the metallic impurity atoms around the nanocavity can be captured in the void during annealing,[134] which implies that metal atoms around nanocavities could enter into nanocavities and be absorbed on the inner surface of nanocavities. In fact, this could be treated as a thermodynamic nucleation process at the nanometer scale,[63] i.e., metallic impurity atoms nucleate on the inner surface of nanocavities. Generally, the Gibbs free energy is an adaptable measure of the energy of a state in the phase transformation among competing phases. From the viewpoint of thermodynamic nucleation theory,[144−148]

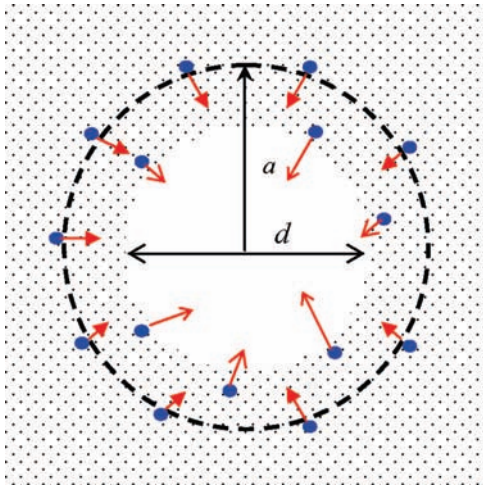

Figure 8. Schematic illustration of a nanocavity in the matrix. d is the diameter of the nanocavity ($d = 2R'$). The dashed circle denotes the radius of the trapping region. Some blue points mean the impurity atoms in the matrix are trapped by the nanocavity.

the Gibbs free energy difference arising from the formation of spherical clusters in the low-pressure gas phase is

$$\Delta G = (\gamma_3(R') - \gamma_2(R'))S_1 + \gamma_1(r)S_2 + \Delta gV \quad (3\text{-}31)$$

where $\gamma_1(r)$, $\gamma_2(R')$, and $\gamma_3(R')$ are the size-dependent nucleus−vapor energy, the inner surface energy of nanocavity−vapor, and the inner surface energy of nanocavity−nucleus interface removal. R' and r are the radii of the nanocavity and nuclei, respectively. S_1 and S_2 are the contact areas of the interfaces of the nucleus−vapor and nucleus−nanocavity, respectively. V is the volume of nucleus, and Δg is the Gibbs free energy difference per unit volume, which is

$$\Delta g = -\frac{RT}{V_s}\ln\left(\frac{p}{p_e}\right) \quad (3\text{-}32)$$

where P_e is the equilibrium vapor pressure of the nucleus and V_s is the mole volume of the nucleus. Considering the additional surface tension induced by the nanoscaled curvatures of the nucleus and nanocavity during the growth process and applying the Laplace−Young equation and Kelvin equation,[149] we can obtain Δg as

$$\Delta g = -\frac{1}{2}\left(\frac{RT}{V_s}\ln\left(\frac{p}{p_e}\right) + \frac{2\gamma_1(r)}{r} + \frac{2\gamma'(R')}{R'}\right) \quad (3\text{-}33)$$

where γ' is the surface free energy of the nucleus with a curvature of R'. Additionally, the surface free energy of the inner surface of a nanocavity with negative curvature evidently shows a size effect according to the above considerations, as is shown in section 3.2.[13] Applying this and calculating the interface area and volume as shown in Figure 8, we obtain

$$S_1 = 2\pi R'(R' - \sqrt{R'^2 - r_0^2}) \quad (3\text{-}34)$$

$$S_2 = 2\pi r(r - \sqrt{r^2 - r_0^2}) \quad (3\text{-}35)$$

$$V = \frac{\pi}{3}\left[r^3(2 + \sqrt{1 - r_0^2/r^2})(1 - \sqrt{1 - r_0^2/r^2})^2 + R'^3(2 + \sqrt{1 - r_0^2/R'^2})(1 - \sqrt{1 - r_0^2/R'^2})^2\right] \quad (3\text{-}36)$$

and

$$r_0 = r\sqrt{1 - \frac{(r + R'\zeta)^2}{R'^2 + r^2 + 2R'r\zeta}} \quad (3\text{-}37)$$

respectively, where ζ is given by

$$\zeta = \cos\theta = \frac{\gamma_2 - \gamma_3}{\gamma_1} \quad (3\text{-}38)$$

in which θ is the contact angle between the spherical cluster and the inner wall of the nanocavity, as shown in Figure 8. Thus, combining eq 3-33 and eqs 3-34, 3-35, and 3-36, we can calculate the Gibbs free energy difference per unit volume for the nucleus.

3.6.3. Diffusion Kinetics Considerations

On the other hand, the kinetic diffusion of metallic impurity atoms in host crystals plays a key role in the process of trapping by nanocavities. We first assume that there is a trapping region created by the nucleation of metal atoms on the inner surface of nanocavities, as shown in Figure 8. Thus, kinetic diffusion is defined to be the random walk of metal atoms from high concentration to low concentration in the host crystals. According to Fick's law, the diffusion of impurity atoms using a spherical coordinate system can be described as follows

$$\frac{\partial C}{\partial t} = D_{\text{iff}}\frac{\partial^2 C}{\partial L_0^2} \quad (3\text{-}39)$$

where C refers to the concentration of impurities, t is the diffusion time, L_0 means the diffusion distance, and D_{iff} represents the diffusion coefficient. In order to solve the equation above, we assume that the concentration of impurity atoms at the inner skin of a nanocavity is zero, while the concentration of impurity atoms at the edge of the trapping region remains constant (c_0) during the diffusion process. Accordingly, one initial condition and one boundary condition are required

$$C|_{L_0=a} = c_0 \ (t \geq 0, 0 \leq \theta \leq \pi, 0 \leq \varphi \leq 2\pi)$$
$$C|_{t=0} = 0 \ (R' \leq L_0 \leq a, 0 \leq \theta \leq \pi, 0 \leq \varphi \leq 2\pi) \quad (3\text{-}40)$$

where a and R' are the radii of the trapping region and the nanocavity, respectively. The solution of eq 3-39 under these conditions would be

$$C(L_0, t) = c_0 + 2c_0\sum_{n=1}^{\infty}(-1)^n\frac{\sin\frac{n\pi L_0}{a}}{\frac{n\pi L_0}{a}}\exp\left[-\left(\frac{n\pi}{a}\right)^2 D_{\text{iff}}t\right] \quad (3\text{-}41)$$

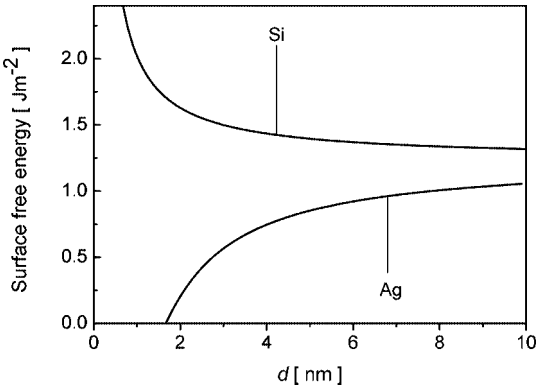

Figure 9. Size-dependent surface free energies of a spherical Ag nanocrystal and a nanocavity in Si at 873 K.

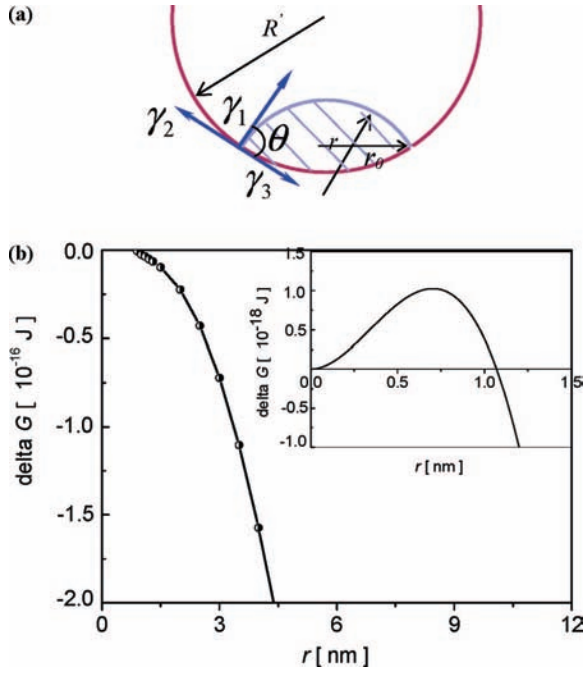

Figure 10. Schematic illustrations of an Ag nucleus on the inner surface of a nanocavity in silicon (a), in which R' and r are the radii of the nanocavity and the nucleation, respectively, and θ is the contact angle. The nucleation Gibbs free energy of Ag on the inner surface of a nanocavity with 10 nm (b), and the inset shows the nucleation Gibbs free energy of impurity atoms in a nanocavity without considerations of the nanosized effect of surface free energy of the inner surface.

Very recently, Ren et al. reported that Ag nanoclusters form in nanocavities in silicon.[122] Therefore, taking the Ag nanoclusters grown in nanocavities in silicon as an example, we treat the trapping behavior of nanocavities toward metallic impurity atoms on the basis of the thermodynamic nucleation and kinetic diffusion mentioned above. In terms of our recent considerations,[12] we calculated the surface free energies of Ag nanocrystals and the inner surface energy of nanocavities in silicon as shown in Figure 9. Clearly, the surface free energy of Ag nanocrystals decreases with decreasing size, while the surface free energy of the inner skin of nanocavities in silicon shows the opposite behavior. Meanwhile, the dependence of the Gibbs free energy of nucleation of metal atoms on the size of nanocavities in silicon based on eq 3-31 is shown in Figure 10. Note that the ratio of P/P_e of Ag evaporation is evaluated from the experimental results based on the Kelvin equation.[25] Surprisingly, the Gibbs free energy of nucleation of metal atoms on the inner surface of nanocavities is negative. This result indicates that the growth of metallic impurity atoms on the inner skin of nanocavities is energetically preferred compared with the same nucleation on the inner surface of nanocavities without consideration of the size-dependent surface energy of the inner skin induced by the negative curvature shown in the inset of Figure 10. In fact, the negative Gibbs free energy of nucleation implies that the contact epitaxy or the inner skin epitaxy of metallic impurity atoms will take place on the inner surface of nanocavities. Therefore, the contact epitaxy of impurity atoms on the inner skin would lead to a trapping effect of nanocavities on the metal atoms around nanocavities. The physical origin of the trapping behavior is that the size-dependent surface energy of the inner surface of nanocavities induced by the large amount of unsaturated chemical bonds at the inner skin can *give* gettering capability to the impurity atoms around nanocavities. Therefore, the nucleation of metal atoms on the inner surface of nanocavities would thermodynamically induce the metal atoms around nanocavities to enter into nanocavities.

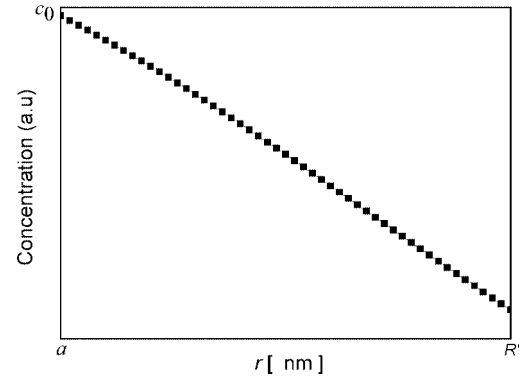

Figure 11. Relationship between concentration of the impurities removed and the diffusion distance in the trapping region.

Figure 11 shows the relationship between the concentration of impurities and the diffusion distance during the diffusion process based on eq 3-41. Evidently, the concentration of impurities decreases as the diffusion distance decreases in the trapping region. This result implies that there is a concentration gradation toward nanocavities of the impurity diffusion flux in the trapping region. In other words, the nanocavities in host crystals act as a sink, and atoms spontaneously flow into nanocavities during annealing, as is shown by experiments.[122,135−138]

On the other hand, diffusion in nanostructures with negative curvature may be important in technological applications such as chemical catalysis. Recently, an interesting experiment addressing the striking enhancement of the catalytic activity for the conversion of CO and H_2 to ethanol by Rh particles confined inside nanotubes was described, and the functions of the densified charge and the very different atomic energy states in the outer and inner surface were accounted for.[150] Indeed, the matter of diffusion and gettering in nanocavities and nanotubes is an interesting topic that will be investigated more deeply in the future.

3.7. Summary

We have addressed in this section the inner surface energy of nanocavities in a host matrix and its effects in yielding anomalous mechanical properties, nonlinear shrinkage behaviors, superheating, and the sink effect from the perspective of nanometer-scale thermodynamics, kinetics, and continuum

mechanics. On the basis of the theoretical predictions above, nonlinear shrinkage behavior and extreme superheating of nanocavities under external thermal activation will take place, and this is confidently expected to be experimentally confirmed. More interestingly, metal impurities could be trapped by nanocavities. Thus, we conclude that introducing a quantity of nanocavities into a host matrix would be an effective way to enhance nanodevice performance. In the following sections, we will apply inner surface energy considerations to other nanostructures with negative curvature, such as nanotubes, nanopores, and shell−core nanoparticles, with an aim toward the predictable design and controllable growth of special nanostructures with programmable functions.

4. Surface Energy of Nanotubes

4.1. Background

As a fundamental building block for nanoelectronic and nano- and micro-optic devices, one-dimensional nanostructures such as wires and tubes have become the focus area in mesoscopic physics, chemistry, and materials science. They not only provide good systems for the investigation of electrical, magnetic, optical, and thermal transport properties due to one-dimensional confinement but also are expected to play a dominant role as both connectors and functional units in promising applications of nanoscale devices.[151−153] Experimentally, many methods have been employed both to synthesize one-dimensional nanostructures and to characterize their related properties.[154] There have been attempts to study the mechanical, thermal, and electrical properties using nanothermodynamics,[155] semiempirical methods,[156] molecular dynamic simulation,[157] ab initio calculations,[158] etc. Compared to nanowires, nanotubes have unique properties and applications. For instance, nanotubes could be regarded as a template to fabricate nanowires or could be filled with various materials. Sun et al. showed that nanotubes can be used as robust nanoscale jigs for extruding and deforming hard nanomaterials.[159] Wang and Yang studied the thermodynamics of the formation of diamond nanowires inside nanotubes.[10] Remarkably, the mechanical properties such as Young's modulus of carbon nanotubes have been reported in a number of theoretical[160−165] as well as experimental[42,166,167] studies. For instance, Cai and co-workers reported that, according to anisotropic continuum theory and finite-element numerical calculations, the Young's modulus decreases significantly as the nanotube diameter is increased.[164] Hsieh and co-workers studied the Young's modulus of single-walled carbon nanotubes and found by molecular dynamics simulations[165] and other methods that it is independent of the tube length but decreases with increasing tube radius. The above theoretical results reveal that the Young's moduli of single-walled carbon nanotubes do have an evident size effect, which is consistent with the corresponding experiments.[165] However, Lu indicated that the Young's modulus of carbon nanotubes is completely insensitive to the tube's size.[162] Hernández et al. predicted that there is a weak dependence of Young's modulus on the tube's size by considering the size-dependent elastic strain energy.[163] In fact, Lu employed an empirical pair potential in his calculations and did not take the curvature-related bonding properties of nanotubes into account.[162] Additionally, Chang and Gao[168] and Shen and Li[169] have systemically studied the elastic modulus of a single-walled carbon nanotube. However, there are not any analytical theoretical tools for the prediction of mechanical properties such as the Young's modulus of nanotubes with a definite wall thickness.

On the other hand, owing to the large ratio of surface-to-volume of nanomaterials, their properties are different from those of the bulk.[120,100,121] Thus, the surface and interface play a significant role in the nature of one-dimensional nanomaterials. Physically, the excess energy associated with surface atoms will significantly influence mechanical behavior in nanostructures.[101] The mechanical behavior of nanotubes is affected not only by elastic strain energy but also by size-dependent atomic bonding energy, which is reflected in the surface free energy. Very recently, Dingreville et al. established for nanoparticles, nanowires, and nanofilms a relationship based on continuum medium mechanics between the surface energy and the mechanical behavior of such nanomaterials.[101] They reported that the effect of surface energy on the mechanical properties of a nanomaterial would be larger than that of the bulk when the characteristic sizes are below 10 nm. Importantly, the surface energy of a nanomaterial has an evident size effect.[12,13] However until now the literature has shed no light on the surface energy of a nanotube, i.e., an inner skin and an outer surface.[100]

In this section, we propose an analytical thermodynamic and continuum medium mechanics approach to elucidate the surface energies of the two surfaces of a nanotube. Importantly, we find the anomalous Young's modulus of a nanotube as induced by size-dependent surface free energy.

4.2. Thermodynamic Analytic Expression of Inner and Outer Surface Energies

The thermodynamic model of the surface energies of the inner and the outer surfaces of a nanotube is established as follows. On the basis of thermodynamic considerations at the nanometer scale,[100] the surface energy of a nanotube is split into the structural part and the chemical part as is shown in eq 3-1. Considering the particular situation of a nanotube with inner and outer surfaces of different curvatures, we can write the size-dependent surface energies of the inner and outer surfaces as

$$\gamma_{\text{inner}} = \gamma_{\text{inner}}^{\text{stru}}(d) + \gamma_{\text{inner}}^{\text{chem}}(d) \tag{4-1}$$

$$\gamma_{\text{outer}} = \gamma_{\text{outer}}^{\text{stru}}(D) + \gamma_{\text{outer}}^{\text{chem}}(D) \tag{4-2}$$

Generally, since the outermost atomic layer is the primary contributor to the surface energy,[62] the surface unit cell is suggested to have four atoms from which to calculate the surface strain energy for a nanocrystal.[170] The schematic illustration of a nanotube with inner diameter d, outer diameter D, and infinite length is shown in Figure 12 a. For the sake of simplification, only one single atomic layer with the surface phase is considered in our case, which is shown as a shell/core/shell structure in Figure 12b. Considering a nanotube with a cubic lattice structure, we take a surface unit cell with four atoms whose coordinates can be showed as (1) (x_i, y_j); (2) (x_{i+1}, y_j); (3) (x_i, y_{j+1}); and (4) (x_{i+1}, y_{j+1}) in Figure 12 c. The elastic strain energy in the surface cell can be written as $U^s_{(i,j)} = U^s_{1-2} + U^s_{1-3} + U^s_{1-4} + U^s_{2-3}$, in which $U^S_{(i,j)}$ represents the deformation energy between atoms i and j due to stretching of the spring. Assuming the surface layer atoms are in relaxation and reconstruction conditions, the atomic positions of 2, 3, and 4 are moved to 2*, 3*, and

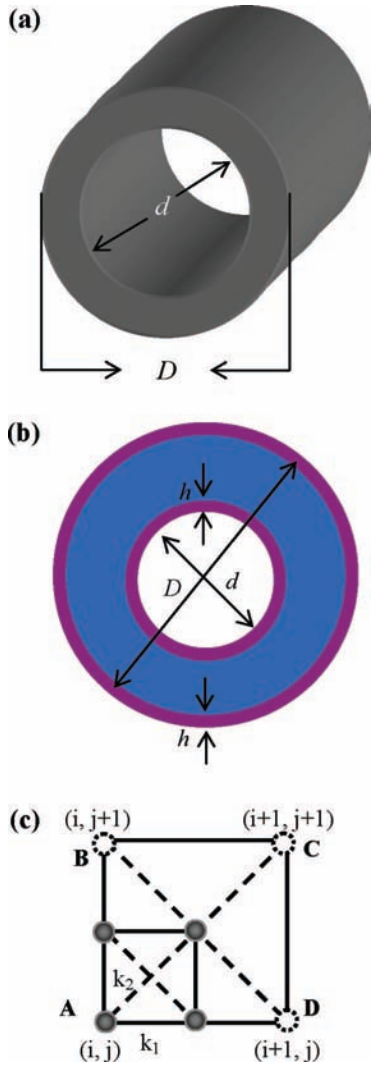

Figure 12. Schematic illustration of nanotube (a) and the shell−core structural model (b). The surface unit cell of a nanotube is shown in (c). *h* is the diameter of an atom, *d* and *D* are the inner and outer diameters of a nanotube, respectively.

and 4*, respectively, for lattice relaxation. Therefore, the total elastic strain energy in a surface unit cell becomes

$$U^s(i,j) = \frac{1}{2}(\omega a^s)^2\{K_1(\varepsilon_x^{s^2} + \varepsilon_y^{s^2}) + K_2[(\varepsilon_x^s + \varepsilon_y^s)^2 + 4\varepsilon_{xy}^{s\ 2}]\} \quad (4\text{-}3)$$

where ω, a^s, ε_i^s ($i = x,y$), and K_j($j = 1, 2$) are the lattice relaxation parameter, the lattice constant of the surface unit cell, the surface atom strain, and the spring coefficients. Thus, the surface strain energy per unit area (S_0) is deduced as

$$\gamma^{\text{stru}} = \frac{U_{i,j}}{S_0} = \frac{1}{2}\{K_1(\varepsilon_x^{s^2} + \varepsilon_y^{s^2}) + K_2[(\varepsilon_x^s + \varepsilon_y^s)^2 + 4\varepsilon_{xy}^{s\ 2}]\} \quad (4\text{-}4)$$

Note that the surface strain ($\varepsilon_{\alpha\beta}^s$ ($\alpha, \beta = 1, 2$)) of a sphere is equal to the bulk strain (ε_{ij} ($i, j = 1, 3$)) under the condition of isotropy by coordinate transformation. Similarly, a nanotube has isotropy, i.e., $\varepsilon_x = \varepsilon_x^s$, $\varepsilon_y = \varepsilon_y^s$, and $\varepsilon_{xy} = 0$. Noticeably, the axial strain is different from the radial strain (the *y* coordinate is the axial direction.). Assuming the axial direction of the nanotube is the {100} plane of the cubic crystal, $\varepsilon_y = \vartheta\varepsilon_x = [(2C_{11})/(C_{11} - 2C_{12})]\varepsilon_x$, in which ϑ is the ratio constant and C_{11} and C_{12} are the elastic constants. The strain in the radial direction is similar to the spherical case based on the liquid drop model,[113,114] i.e., $\varepsilon_x = \mp[(2k)/(3d)]\sqrt{(d_0 h S_{\text{mb}} H_{\text{mb}})/(kV_s R)}$, in which *k*, *h*, and d_0 denote the compressibility of bulk crystals, the atomic diameter, and the critical diameter in 3*h* of nanotube.

On the other hand, the chemical contribution γ^{chem} of the nanotube inner and outer surfaces is similar to those of the nanocavity and nanocrystal. Physically, the chemical part of surface free energy (γ_0^{chem}) can be given by $\gamma_0^{\text{chem}} = (1 - \sqrt{z_s/z_b})E_b$, where z_s, z_b, and E_b are the surface and bulk coordination number and the cohesive energy, respectively.[171,172] Remarkably, the atomic cohesive energy has an evident size effect, as is confirmed by related experiments and theoretical calculations.[50,173−175] Kim et al. found by measuring the oxidation enthalpy of nanocrystals that the atomic cohesive energy of Mo and W are dependent on size.[173] Sun also suggested based on the BOLS correlation mechanism that the E_b increases with decreasing size.[174] In addition, Jiang et al. proposed size dependence of the cohesive energy for nanocrystals.[175] Overall, due to the large ratio of surface-to-volume for nanostructures, the energetic state of atoms at the surface or interface is very different from the counterpart trunk. Therefore, the chemical contributions of surface energies of inner and outer surfaces of nanotube can be deduced to be

$$\gamma_{\text{inner}}^{\text{chem}}(d) = \gamma_0^{\text{chem}}\left(1 + \frac{4h}{d}\right) \quad (4\text{-}5)$$

$$\gamma_{\text{outer}}^{\text{chem}}(D) = \gamma_0^{\text{chem}}\left(1 - \frac{1}{D/D_0 - 1}\right)\exp\left(-\frac{2S_{\text{mb}}}{3R}\frac{1}{D/D_0 - 1}\right) \quad (4\text{-}6)$$

where γ_0^{chem} is the value in the plane surface with 0 curvature.

4.3. Novel Mechanical Behaviors Induced by Surface Energy

Mechanically, there are three stiffness parameters that need to be addressed in a deformation analysis of the equivalent beam on the basis of structural mechanics.[176,177] In detail, these three stiffness parameters are expressed as the flexural rigidity *EI*, the tensile resistance *EA*, and the tensional stiffness *G′J*, where *E*, *G′*, *A*, and *J* denote the Young's modulus, shear modulus, cross-sectional area, and polar inertia of the beam. However, due to the high surface-to-volume ratio of nanotubes, the flexural deformation at the surfaces will sustain the largest stresses and strains under the condition of vibrational cases. As a result, the surface elasticity plays a more important role in the effective stiffness than an axial deformation does. As the significant quantity relevant to the inner and outer surface state, the flexural rigidity *EI* is an appropriate quantity to characterize the axial mechanical properties of a nanotube based on the above considerations. Very recently, Chen et al. defined the product *EI* as the effective flexural rigidity parameter governing the axial deformation of ZnO nanowires, with *E* being the effective Young's modulus in the axial direction and *I* being the moment of inertia.[154] Also, for the spherical nanocrystal case, the effective flexural rigidity along the diameter can be expressed as $EI = E_0I_0 + E_sI_s$, where the subscripts 0 and *s* denote the core and the shell, respectively. Thus, the

effective Young's modulus in the axial direction can be given by $(E/E_0) = [1 - (2h/D)]^5 + (E_s/E_0)(5/3)[(6h/D) - (12h^2/D^2) + (8h^3/D^3)]$.[121]

Similarly, the size-dependent elastic properties of nanotubes can be expressed in terms of the shell/core/shell structure shown in Figure 12b. Therefore, neglecting the shear modulus, the effective flexural rigidity in the axial direction of nanotubes can be defined as

$$EI = E_0 I_0 + E_s^{\text{in}} I_{\text{in}} + E_s^{\text{out}} I_{\text{out}} \tag{4-7}$$

where E_0, E_s^{in}, and E_s^{out} denote the Young's modulus of the nanotube in the core and the inner and outer shells, respectively. I_0, I_{in}, and I_{out} are the moments of inertia again in the core and the inner and outer shells, respectively. Substituting I_0, I_{in}, and I_{out} into eq 4-7, we can obtain

$$E = E_0\left[1 + \frac{24h^2(D^2 - d^2) - 8h(D^3 + d^3) - 32h^3(D + d)}{D^4 - d^4} + \frac{E_s^{\text{in}}}{E_0}\frac{(16h^4 + 24d^2h^2 + 8d^3h + 32dh^3)}{D^4 - d^4} + \frac{E_s^{\text{out}}}{E_0}\frac{(-16h^4 - 24D^2h^2 + 8D^3h + 32Dh^3)}{D^4 - d^4}\right] \tag{4-8}$$

In addition, the surface Young's modulus (E_s) in the inner and outer shells can be deduced based on the recent BOLS considerations to be[178]

$$\Delta E/E_0 = (E_s - E_0)/E_0 = (a_s/a_0)^{-m} - 3a_s/a_0 + 2 \tag{4-9}$$

where m is a characterization parameter of the bond nature. For compounds and alloys $m = 4$, and for a metal $m = 1$. Therefore, $(E_s)/(E_0) = 3 - 2(a_s)/(a_0)$ for metals and semiconductors. The surface lattice constant (a_s) in the axial direction for a nanotube is different from that for the bulk. The nanotube will be in the self-equilibrium state, and a_s takes the form

$$a_s = a_0\left(1 - \frac{4\gamma}{d}\Xi'\right) \tag{4-10}$$

with

$$\Xi' = \frac{C_{11}}{(C_{11} + 2C_{12})(C_{11} - C_{12})}$$

where Ξ' is the orientation-dependent constant for the nanotube. According to the above analysis, the relationship between the Young's modulus and the surface energy can be obtained as

$$\frac{E_s}{E_0} = 3 - 2\left(1 - \frac{4\gamma}{d}\Xi'\right) \tag{4-11}$$

Therefore, we can obtain the effective Young's modulus of a nanotube as

$$E = E_0\left[1 + \frac{24h^2(D^2 - d^2) - 8h(D^3 + d^3) - 32h^3(D + d)}{D^4 - d^4} + \frac{(16h^4 + 24d^2h^2 + 8d^3h + 32dh^3)}{D^4 - d^4}\left(3 - 2\left(1 - \frac{4\gamma^{\text{inner}}(d)}{d}\Xi'\right)\right) + \frac{(-16h^4 - 24D^2h^2 + 8D^3h + 32Dh^3)}{D^4 - d^4} \times \left(3 - 2\left(1 - \frac{4\gamma^{\text{outer}}(D)}{D}\Xi'\right)\right)\right] \tag{4-12}$$

On the basis of the model established above, we calculate the surface energy and the effective Young's modulus in the axial direction of a copper nanotube. The variations of the surface energy of a nanotube are plotted in Figure 13. Clearly, the surface energy of the inner surface of a nanotube increases and the surface energy of the outer surface decreases with decreasing diameter of the nanotube. However, when $D > 10$ nm, the surface energies of both the inner and outer surface go smoothly to that of the bulk. These results show that the size of 5 nm seems to be a threshold value to the size-dependence of copper nanotubes.

Note that, on the inner surface of a nanotube, both the density of the elastic strain energy of lattice relaxation and the density of dangling bonds become large with decreasing diameter. Additionally, on the outer surface of a nanotube, the total contribution of the structural and chemical parts leads to a decrease of the surface energy with decreasing size. Importantly, the surface energy is dependent on the surface lattice structure through the variation of the coordination number of atoms for a specific atomic site. For example, in the case of carbon nanotube walls, we could select the hexagonal unit cell to calculate the surface elastic energy (γ^{stru}) and surface chemical energy (γ^{chem}), and from those the relevant properties could be evaluated.

Figure 14 shows the relationship between the ratio of the effective Young's modulus of a nanotube and the bulk according to eq 4-12 at a constant thickness of 1 and 2 nm, respectively. The value of E/E_0 smoothly increases with decreasing diameter of the nanotube. Interestingly, the effective Young's modulus of a nanotube with small thickness is larger than that of a nanotube with large thickness. When $D \rightarrow \infty$, the ratio (E/E_0) goes to 1, which means the effective Young's modulus of a nanotube will be equal to that of the bulk. Interestingly, the above results agree well with the molecular dynamics simulations by Hsieh et al.[160] Furthermore, we can obtain the effective Young's modulus of nanotubes with constant outer diameters of 5, 10, and 20 nm and various inner sizes as shown in Figure 15. The variant trend in the small nanotube becomes much larger than that of the large one. Additionally, the thinner the nanotube is, the larger is the effective Young's modulus. Tu et al.,[44] using the local density approximation model, investigated single-walled carbon nanotubes and multiwalled carbon nanotubes as elastic tubes with the effective Young's modulus dependent on the number of layers. They reported a Young's modulus of $E = 4.7$ TPa if the number of atomic layers $N = 1$, which corresponds to a single-walled carbon nanotube, and $E = 1.04$ TPa if $N \gg 1$, which is just the Young's modulus of bulk graphite. The intrinsic bulk modulus [K] for nanowires with $\gamma = 1.24$, 1.4, and 2.0 J/m^2 can be read at each particle size from Figure 4 as the vertical coordinate

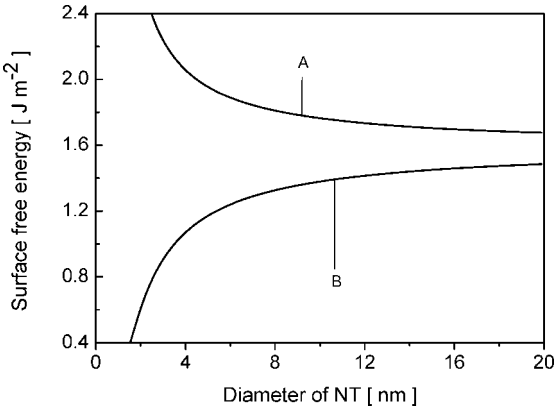

Figure 13. Dependence of surface energy of nanotube on the diameter. The curve (A) is in the inner surface, while the curve (B) is in the outer surface. The elastic parameters are $C_{11} = 167.38$ GPa and $C_{12} = 124.11$ GPa.[101]

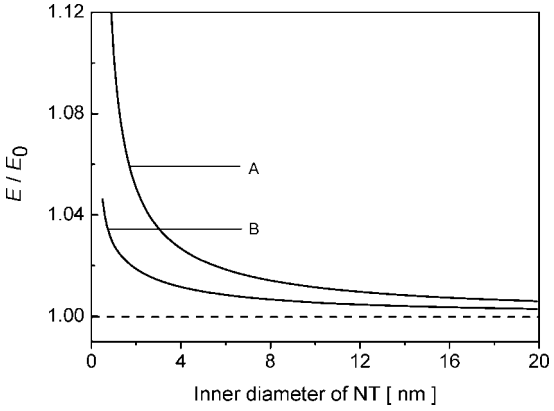

Figure 14. Relationship between the ratio of E/E_0 and the diameter of nanotube. The thickness of nanotube is assumed at 1 nm in (A) and 2 nm in (B).

for that particle size of the corresponding curve, A, B, or C, respectively. Thus, the Young's modulus of nanowires increases with decreasing nanowire diameter. Experimentally, Chen et al.[154] reported that the size-dependent Young's modulus in the [0001] orientation of ZnO nanowires increases significantly with decreasing diameter. Therefore, our theoretical results definitely show that, for the same material, the effective Young's modulus of a nanotube is higher than that of a nanowire of the same size, and the effective Young's modulus of both a nanotube and a nanowire are higher than that of the bulk material. The physical origin of this effect is the size-dependent surface energy of nanostructures.

4.4. Mechanical Properties of Nanoporous Structural Materials

Nanoporous structures have become the focus of intensive research in recent years due to their unique applications in mesoscopic physics and chemistry, and their potential applications in technologies including sensing, catalysis, and DNA translocation. They may also serve as templates for nanostructure self-assembly.[179−184] Meanwhile, the study of nanoporous materials such as nanopores, nanocavities, and nanochannel-arrays can afford a deep understanding of the new scientific results for such useful systems with negative surface curvature. Because the number of atoms near the inner surface in nanoporous structures is very large compared to the total number of atoms, surface effects can dominate

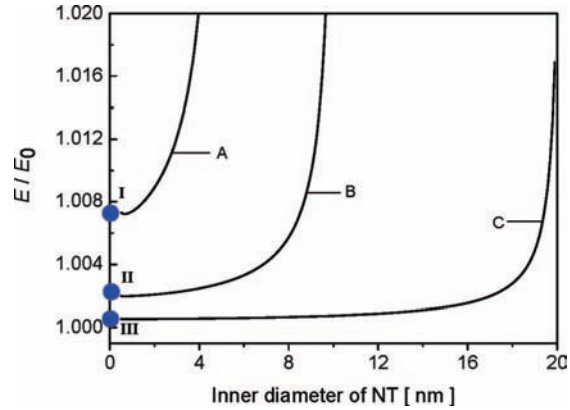

Figure 15. Dependence of Young's modulus of nanotube on D: $D = 5$ nm in (A), $D = 10$ nm in (B), and $D = 20$ nm in (C). The blue dots with I, II, and III denote the corresponding value of nanowires.

the physical and chemical properties. It is well-known that many physical properties of nanomaterials and nanostructures, including melting temperature, surface free energy, elastic modulus, and cohesive energy, show strong size effects. The nanoporous materials with large internal surface area have, compared with other nanomaterials, been extensively employed as good host materials in nanotechnology.[185] For example, nanopores and nanocavities show a novel sink effect in capturing other molecules, and the effect can be controlled by tuning the pore size and porosity.[180]

Since the reduced coordination of atoms of nanoporous structures can lead to the redistribution of electronic charge and change the cohesive energy of single atoms in a matrix, their mechanical responses differ from those of atoms in the bulk counterpart. Additionally, the mechanical applications of nanoporous structures are currently an important subject of much research. Thus, numerous expressions concerning the porosity-dependence of the isotropic elastic modulus have been developed using effective medium theory.[186,187] The effective elastic modulus is suitable for describing the mechanical properties of nanoporous structures. In general, the effective elastic modulus of a porous material is expressed in terms of the elastic moduli of the matrix and the porous inclusion in the material.[188] However, the surface elasticity of nanostructures is different from the bulk, which is generalized by the Young−Laplace equation based on the mechanical equilibrium principle.[189] Dual et al. have pointed out that the stiffness of nanoporous materials may be made to exceed that of the nonporous counterpart bulk by satisfying certain surface modifications.[190] In fact, nanoporous structures are similar to nanocavities in having negative curvature of their inner surface in the matrix. The large inner surface energy can lead to the effective elastic modulus of the negative curvature surface being larger than that of the plane case.[40] Importantly, the inner skin of nanocavities will undergo local hardening by local bond stiffening around nanocavities when the void size becomes small.[13,40] However, there are not any quantitative theories to predict the mechanical responses of nanoporous structures when the cylindrical pore size is in the range of several nanometers.[180] In this section, we propose a theory that quantifies the stiffening of nanoporous structures and shows that the effective bulk elastic modulus of nanoporous structures is determined by the cylindrical pore size and porosity.

A model constructed for nanoporous structures is shown in Figure 16. In fact, the physical properties of the inner

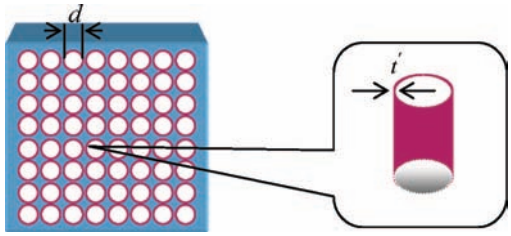

Figure 16. Schematic illustration of nanoporous structures. d is the diameter of a cylindrical pore. t' is the thickness of the inner surface. The inset is an arbitrary cylindrical nanopore in nanoporous structure.

surface of nanopores are the same as those for nanotubes. Meanwhile, the inner skin of nanopores differs from the bulk counterpart because of the negative curvature. Thermodynamically, the inner surface free energy originates from the atomic bonding energy and the elastic strain energy of the inner surface of nanoporous structures.[191]

With decreasing size of the nanoporous structures, their negative curvature induces a steady increase of the density of the atomic bonds. Similarly, the density of the elastic strain energy increases as the cylindrical pore size decreases. Thus, in terms of our previous considerations,[170] the inner surface free energy (γ) of a cylindrical pore in nanoporous structures can be written as $\gamma = \gamma^{\text{stru}} + \gamma^{\text{chem}}$, where γ^{stru} is the structural contribution induced by the elastic strain energy of the inner surface atoms, while γ^{chem} arises from the cohesive energy of the surface atoms based on the broken bond rule, which is deduced as $\gamma(d) = \gamma_0(1 + 4h/d) + \bar{\alpha}\varepsilon^2$, where γ_0 and d are the value in the plane surface with zero curvature and the diameter of a cylindrical nanopore in the matrix, respectively, as is shown in Figure 12. ε is the lattice strain of the inner skin. The relaxation and reconstruction of the inner skin atoms of nanoporous structures can cause the inner shell to be more stiffened than before. Generally, a bond broken at the inner surface of a nanoporous structure will cause the remaining bonds of the undercoordinated atoms to contract spontaneously. Meanwhile, the bond strength is stronger than that in bulk. Thus, the surface Young's modulus (E^s_{np}) in the inner shell can be calculated based on eqs 2-4−2-9, i.e., $\Delta E/E_0 = (E^s_{\text{np}} - E_0)/E_0 = (a_s/a_0)^{-m} - 3a_s/a_0 + 2$,[57] where E_0 is the Young's modulus in bulk. The surface atomic strain in the self-equilibrium state can be derived as $\partial U_{\text{tot}}/V_0\partial\varepsilon|_{\varepsilon=\hat{\varepsilon}} = 0$, where U_{tot} denotes the total strain energy in unit volume (V_0) of nanoporous structures. Assuming the isotropic state in our case, the relationship between the surface lattice constant and the surface free energy in nanoporous structures in the self-equilibrium state can be deduced to be

$$a_s = a_0\left(1 - \frac{4\gamma(d)}{d}\Xi'\right) \tag{4-13}$$

Therefore, the inner surface Young's modulus can be expressed as the size function

$$E^s_{\text{np}} = E_0\left(3 - 2\left(1 - \frac{4\gamma(d)}{d}\Xi'\right)\right) \tag{4-14}$$

Assuming that the matrix and the inner surface of the cylindrical pores are both isotropic,[192] the Lamé elastic parameters at the surface can be calculated as

$$\lambda^s = E_0\left(3 - 2\left(1 - \frac{4\gamma(d)}{d}\Xi'\right)\right)\frac{\nu\, t'}{(1-\nu)(1-2\nu)} \tag{4-15}$$

$$\mu^s = E_0\left(3 - 2\left(1 - \frac{4\gamma(d)}{d}\Xi'\right)\right)\frac{t'}{2(1+\nu)} \tag{4-16}$$

where t' is the thickness of the surface layer in the nanoporous structure. ν is the Poisson's ratio. Furthermore, the surface constitutive equation can be written based on Hooke's law:

$$\sigma = \lambda_s(tr\varepsilon^s)1 + 2\mu_s\varepsilon^s \tag{4-17}$$

where σ is the surface stress tensor. 1 is the second-order unit tensor in the two-dimensional space. λ_s and μ_s are the surface elastic constants for the isotropic surface. According to the generalized self-consistent method (GSAM),[190,193] we employ the nonvanishing strain components with a cylindrical coordinate system. The transverse bulk elastic modulus k_e can be determined from the boundary conditions and the displacement solutions, which are expressed as $u^0_r = \varepsilon^0_m r$, $u^0_\phi = 0$, $u^0_z = 0$, $u^i_r = a_i r + (b_i)/(r)$, $u^i_z = 0$, and $u^i_\phi = 0$, where r is the radius of nanopore, and i (i = m, e) denotes the matrix and the effective medium, respectively. It is found that the k_e for nanoporous structures is given by

$$\frac{k_e}{k} = \frac{(1-2\nu)[2(1-p_{or}) + (1+p_{or}-2p_{or}\nu)((2\lambda^s + 4\mu^s)/(d\mu_m))]}{2(1+p_{or}-2\nu) + (1-p_{or})(1-2\nu)((2\lambda^s + 4\mu^s)/(d\mu_m))} \tag{4-18}$$

where k, μ_m, and p_{or} are the bulk elastic modulus, the shear modulus, and the porosity of nanoporous structures, respectively. Combining eqs 4-15, 4-16, and 4-18, we can obtain the porosity- and size-dependent effective bulk elastic modulus of nanoporous structures.

On the basis of the established model mentioned above, we calculate the inner surface free energy, the surface Young's modulus, and the effective bulk elastic modulus of Au nanoporous structures. Clearly, the inner surface free energy of Au nanoporous structures becomes large with decreasing diameter, as is shown in Figure 17a. Interestingly, when $d > 5$ nm, the surface free energy of the inner surface goes smoothly to that of the bulk. Physically, this is attributed to the density of the lattice relaxation of elastic strain energy and the density of dangling atomic bonds both becoming large with the decreasing pore size. In addition, the variations of E^s_{np} for Au nanoporous structures are plotted in Figure 17b. It can be seen that the inner surface Young's modulus of Au nanopores increases with decreasing pore diameter. Similarly, when $d > 5$ nm, E^s_{np} goes smoothly to that of the bulk. Thus, 5 nm seems to be a threshold value for the size dependence of Au nanopores. Indeed, the state of undercoordinated atoms in the inner skin in nanoporous structures would be different from that in the bulk, which is similar to the case for nanowires.[154] The surface layers of nanowires can be approached as a composite wire with a shell−core structure that is composed of a cylinder core in bulk and a shell in surface layer coaxial with the core. Thus, the surface Young's modulus would be higher than that of the core bulk. In our case, nanoporous structures can be treated as an inner shell−outer core structure.

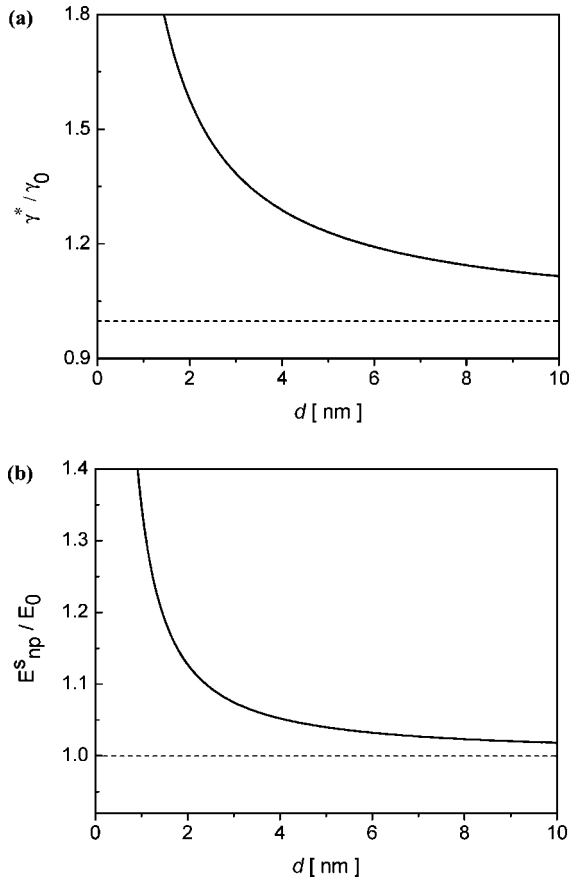

Figure 17. Size-dependent inner surface free energy (a) and surface Young's modulus (b) of Au nanoporous structures.

According to eq 4-18, the relationship among the cylindrical pore size, the porosity, and the ratio of the effective bulk elastic modulus of nanoporous structures and bulk at the constant porosity of 0.1, 0.2, and 0.3 is shown in Figure 3, respectively. Clearly, the value of k_e/k increases smoothly with decreasing diameter of the nanoporous structures. The effective bulk elastic modulus of nanoporous structures with small cylindrical pore size is larger than that of nanoporous structures with large cylindrical pore size. Very recently, Mathur et al.[37] reported experiments showing that the effective Young's modulus of Au nanoporous leaf shows a strong size effect, i.e., the modulus increases with decreasing ligament size in the range of 3−40 nm. Thus, our theoretical predictions do depict the trend of mechanical responses. When $p \rightarrow 1$, the ratio (k_e/k) goes to 0. Furthermore, at constant cylindrical pore sizes of 1, 2, 5, and 8 nm, we can obtain the effective bulk elastic modulus of Au nanoporous structures with various porosities, as is shown in Figure 18. The variant trend in the Au nanoporous structures with a small pore size becomes higher than that of one with a large pore size. Surprisingly, the bulk elastic modulus of nanoporous structures with cylindrical pore size of less than 2 nm exhibits the stiffening effect shown in Figure 19. In other words, the effective bulk elastic modulus of nanoporous structures with a pore size of less than 2 nm is larger than that of the bulk counterpart. These theoretical results are consistent with the recent predictions.[190]

It is interesting to note that a certain number of defects such as atomic vacancies or point defects could enhance the mechanical strength of solid specimens.[194] Wu et al.[195] demonstrated that the hollow polymer nanofibers show the large axial stiffening effect and found that the fiber diameter has an evident effect on the mechanical response of nanofibers. Similarly, the hardness of FeAlN and WAlC is directly correlated with the concentration of nitrogen and carbon vacancies.[196,197] In particular, Biener et al.[36] demonstrated that the enhancement of the hardness of metal foams can reduce the length scale of ligaments and pores. Moreover, nanoporous Au has a strength some 10 times higher than that of micrometer-sized porous structures.[198] Accordingly, the mechanical strength of solid specimens could be enhanced by the introduction of atomic vacancies, nanocavities, or nanopores. Importantly, the experimental results above are quite consistent with the theoretical predictions in this study.

In fact, the surface energy of nanoporous structures plays a significant role in their mechanical properties. The elastic responses of materials, a fundamental physical property, can be understood and predicted from the size effect in the mechanical properties of nanomaterials. Generally, for nanomaterials such as nanoparticles, nanowires, and nanofilms, the effect of surface energy on the mechanical responses are possibly enhanced when the characteristic sizes are below 10 nm.[101] Combining eqs 4-14, 4-15, and 4-16, we can anticipate that local stiffening will take place around the cylindrical pore skin because of the size-dependent surface energy of the inner skin. In other words, the inner surface energy of nanoporous structures increases monotonically as the diameter of the pore decreases down to around 2 nm. In contrast, the stiffening of nanoporous structures is smaller than that of nonporous materials when the size and porosity are beyond the critical size.

Actually, other causes may also induce the stiffening effect in nanoporous structures. Parida et al.[199] reported a macroscopic reduction by up to 30% in the volume of Au nanoporous leaf during dealloying. A large number of dislocations and defects appear during the Au nanoporous leaf formation. According to the effective medium theory, the effective elastic modulus would become large, because of the rapidly increasing relative density.

4.5. Summary

It is understood that the difference between the energy state in the inner skin and outer surface of nanotubes determines the physical properties. Also, for nanoporous structures, the effective bulk elastic modulus is higher for nanoporous structures with pore size less than 2 nm than for the nonporous materials. Note that the porosity and the size of the cylindrical pores plays the most significant role in the stiffening of nanoporous structures. Importantly, the approach developed is in good accord with existing models based on the semiempirical method and ab initio calculations. A combination of these models should provide deeper insight into the physical and chemical origins and the general trends of the mechanical behavior of nanostructures with negative curvature. Additionally, consistency between theoretical predictions and experimental measurements on the mechanical properties of the nanotubes and nanopores considered gives evidence for the validity of the current approach. Thus, we expect the established models to be generally applicable to the mechanical responses of nanomaterials with structures having negative curvature.

5. Surface Energy of Shell−Core Nanostructures

5.1. Observations

Recently, shell−core bimetallic nanostructures have attracted great interest because of their outstanding physical and chemical natures, such as the controllable growth of quantum dots and the fabrication of nanoscaled devices.[25,200,201] In the past several decades, many methods have been developed to create shell−core bimetallic nanostructures. However, the enormous ratio of the surface area to mass of these shell−core nanostructures creates additional excess free energy comparable to that of the lattice energy of the bulk material, which leads to instability of the interface or surface.[202] Most strikingly, in shell−core bimetallic nanoparticles, interfacial alloying induced by the size-dependent interface free energy and heat of alloy formation can occur.[28,30−32,112] It should be noted that the spontaneous interfacial alloying in shell−core nanoparticles at ambient room temperature definitely differs from the alloying by the solid-state reaction at moderate annealing temperatures (∼500 °C) reported by Schwarz and Johnson in 1983.[203] The solid-state reaction is achieved thermodynamically by thermal activation at a moderate temperature. In other words, the thermal annealing drives the interfacial reaction between metallic layers. However, Meisei's experiments clearly indicate that the size effect from shell−core nanoparticles seems to be responsible for the spontaneous interfacial alloying.[28] Since the spontaneous alloying takes place at ambient temperature without any external thermal activation, the thermodynamic driving force causing the interfacial alloying must result from the nanometer-sized confinement in shell−core structures. Therefore, the alloying by the solid-state reaction is actually driven by external thermal activation and is not really spontaneous. Additionally, Lin and coworkers developed a thermodynamic model to elucidate the alloying in immiscible binary metallic multilayers upon the solid-state reaction by thermal activation at a moderate temperature.[204,205] However, the mechanism for the spontaneous interfacial alloying of shell−core bimetallic nanostructures is currently still not clear. There is especially much less theoretical understanding of the basic physical and chemical factors. For instance, what is the mechanism of the size-dependent rate of alloying for the interfacial alloying occurring in Au−Ag nanoparticles? Why does the alloying stop beyond the *buried* interface rather than proceed to a completely random alloy?[28] In this section, in order to pursue these issues, we have derived the theoretical size-dependent thermodynamics and size-dependent kinetics for spontaneous interfacial alloying in shell−core nanoparticles. In the thermodynamic approach, we study only the driving force causing the interfacial alloying by developing a size-dependent model of the mixing enthalpy and interfacial energy of a bimetallic shell−core structure. In the kinetic approach, we explain the unusual interfacial diffusion behavior on the basis of the proposed size-dependent kinetic diffusion model. In both approaches, we assume on the basis of Nanda's experiments that the nanoparticles are spherical and isotropic.[25] However, at the atomic scale, Baletto and Ferrando reported that the structure of nanoclusters could change with size and be anisotropic and of polyhedral shape.[206] Further, the different sizes and structures of nanoclusters can engender internal strain.[207,208] However, Hudgins et al. considered clusters as quasispherical for the number of atoms greater than about 25, even if they do not form crystalline structures at these sizes.[209]

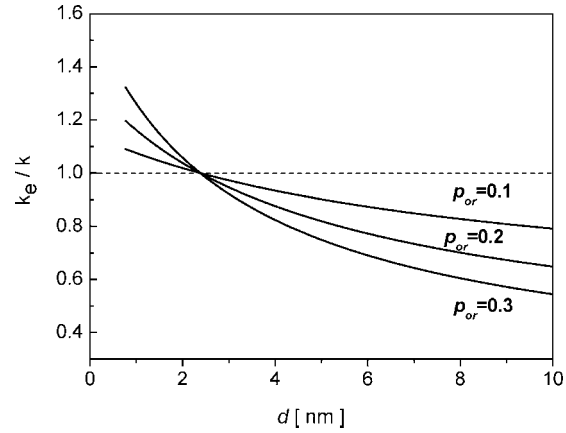

Figure 18. Dependence of the effective bulk elastic modulus of Au nanoporous structures on the diameter and the porosity.

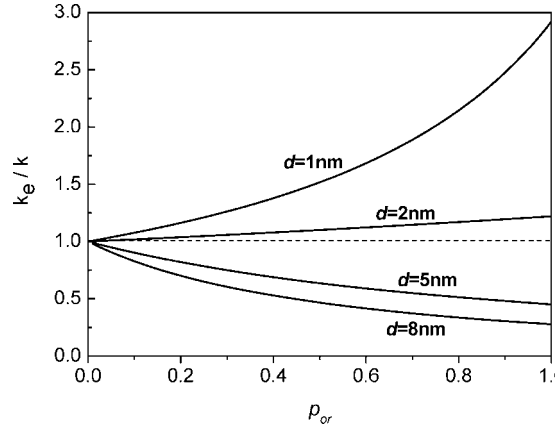

Figure 19. Relationship among the effective bulk elastic modulus and the porosity and the diameter.

According to thermodynamics, layered structures are found in a number of applications ranging from magnetic to structural, and the stability of the interface is often critical to the performance of these materials since the interface must resist coarsening and breakdown, such as interfacial alloying, which is driven thermodynamically by the free energy of interfaces.[204] Therefore, understanding the thermodynamic driving force for interface degradation in layered structures is of major technological importance. In fact, a shell−core particle is a bilayered structure. For miscible systems, the thermodynamic driving forces causing the interfacial alloying in layered structures include the negative mixing enthalpy and the interface free energy. Further, when the thickness of the interfacial alloying in the bimetallic bilayer is limited to several nanometers, the thermodynamic driving force is mainly from the negative mixing enthalpy and interface energy of the system.[205,210] Therefore, we address the interfacial alloying in bimetallic miscible shell−core layered structures. A schematic illustration of a general shell−core nanoparticle with binary metallic components A and B is shown in Figure 20, in which we define the structure for the core A and the shell B and the interfacial alloying layer with thickness L nm. In the following section, we deduce from theory the analytic expression for the size-dependent thermodynamic driving force, which causes interfacial alloying in a shell−core structure.

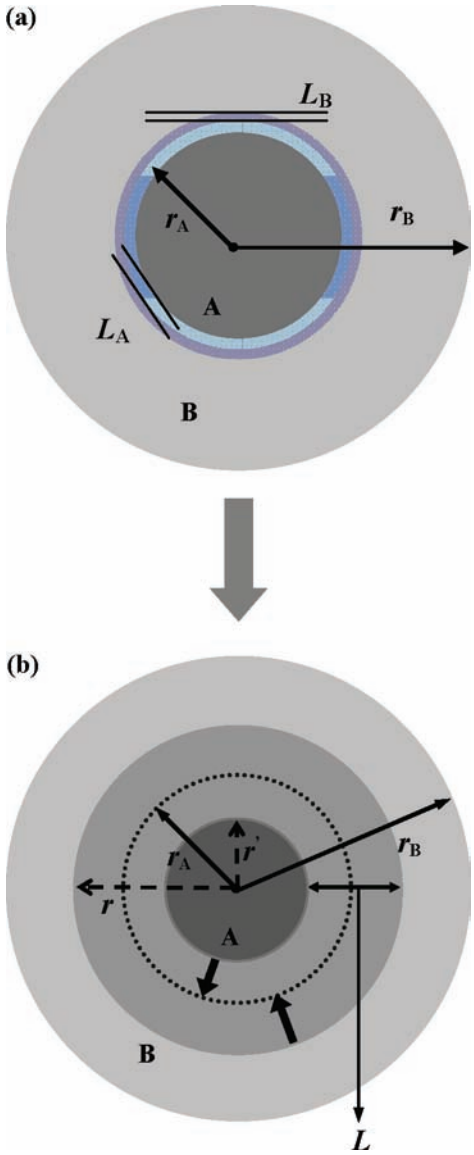

Figure 20. Schematic illustration of the shell−core nanostructure with binary metallic composed of component of A and B, (a) before alloying and (b) after alloying.

5.2. Thermodynamic Analytic Expression of Shell−Core Nanostructures

Interfacial interactions, symmetry breaking, structural frustration, confinement-induced entropy loss, etc., can all play key roles in determining atomic assembly of a nanosystem in a physically confined environment. So, the interfacial free energy is an important physical quantity in multilayered films. Buff demonstrated the liquid−gas interfacial free energy as related to size dependence in 1951.[105] Also, Jiang et al. reported that the interface energy between the solid and vapor varies with the dimension of the nanocrystals.[104] Thus, the size-dependent solid−solid interface free energy in binary shell−core structures is deduced as follows.

For a shell−core interface with a spherical particle diameter d, the surface energy of component A can be deduced as in the similar case for nanocrystals. In a similar manner, the following expression is obtained based on eq 3-1, i.e., $\gamma_A = \gamma_A^{chem} + \gamma_A^{stru}$. Thus, we have

$$\gamma_A^{chem} = \gamma_{(hkl)}\left(1 - \frac{1}{D_A/D_{A0} - 1}\right)\exp\left(-\frac{2S_{mb}}{3R}\frac{1}{D_A/D_{A_0} - 1}\right) \quad (4\text{-}20)$$

$$\gamma_A^{stru} = \frac{1}{2}\{\alpha_1(\varepsilon_x^{s^2} + \varepsilon_y^{s^2}) + \alpha_2[(\varepsilon_x^s + \varepsilon_y^s)^2 + 4\varepsilon_{xy}^{s\ 2}]\} \quad (4\text{-}21)$$

The surface strain ($\varepsilon_{\alpha\beta}^s$) of a sphere is related to the absolute bulk strain (ε_{ij}) within the particle through a coordinate transformation $\varepsilon_{\alpha\beta}^s = t_{\alpha i}t_{\beta j}\varepsilon_{ij}$, in which α,β range from 1 to 2 and i, j range from 1 to 3. The $t_{\alpha i}$ is transformation tensor, and the transformation matrix for cubic structure metals is expressed as in eq 4-22.

$$[t_{ij}] = \begin{bmatrix} \cos\theta\cos\phi & \sin\theta\cos\phi & -\sin\phi \\ -\sin\theta & \cos\theta & 0 \\ \sin\phi\cos\theta & \sin\phi\sin\theta & \cos\phi \end{bmatrix} \quad (4\text{-}22)$$

Note that D_0 is the smallest size with $D_0 = 3h$ for spherical particles.

On the other hand, it can also readily be demonstrated that, in the case of the surface energy in the inner wall of component B, the equation has the form: $\gamma_B = \gamma_B^{chem} + \gamma_B^{stru}$. Likewise, we have

$$\gamma_B^{chem} = \gamma_{B0}\left(1 + \frac{4h}{d}\right) \quad (4\text{-}23)$$

$$\gamma_B^{stru} = \varepsilon^2\bar{\alpha} \quad (4\text{-}24)$$

Thus, we conclude that the average interface free energy $\bar{\gamma}'$ between components A and B is found to be

$$\bar{\gamma}' = (\gamma_A + \gamma_B)/2 \quad (4\text{-}25)$$

Thus, the interface energy in the shell−core structure is definitely size dependent.

5.3. Spontaneous Interfacial Alloying

Generally speaking, the thermodynamic driving force that can lead to interfacial alloying in mutilayers includes the interface free energy and the heat of mixing. It is notable that the size-dependent melting enthalpy of nanoparticles has been derived using several models.[211] Similarly, for the formation or mixing enthalpy $H_f(L)$ of bimetallic systems, the size-dependent $H_m(L)$ function can first be expressed by $H_m(L) = H_{m_b}\exp[(-2S_{m_b})/(3R)(1)/(L/L_0 - 1)][1 - (1)/(L/L_0 - 1)]$ where $T_m(L)$, $S_m(L)$, and $H_m(L)$ are the size-dependent melting temperature, the melting entropy, and the melting enthalpy,[212] respectively. S_{m_b}, H_{m_b}, and T_{m_b} are the corresponding bulk values. Therefore, for nanocompounds with two different metallic elements, the formation enthalpy $H_f(L)$ should be size dependent. L is the thickness of the mixing or alloying layer with L_0' being the critical thickness. Accordingly, for binary nanocompounds, the size-dependent formation enthalpy is defined as following

$$H_f(L) = H_{f_b}\exp\left(\frac{-2S_{f_b}}{3R}\frac{1}{L/L_0' - 1}\right)\left(1 - \frac{1}{L/L_0' - 1}\right) \quad (4\text{-}26)$$

where S_{f_b} is the bulk mixing entropy with $S_{f_b} = -R(X_A \ln X_A + X_B \ln X_B)$, in which X_i (i = A, B) denote the atomic percentage of components. Note that for miscible bimetallic systems, the heat of formation is negative, whereas it is positive in immiscible systems. Finally, combining eqs 4-25 and 4-26, we obtain the size-dependent thermodynamic driving force, ΔF, for interfacial alloying in a shell−core structure as in eq 4-27.

$$\Delta F = S_f\bar{\gamma} - H_f(L) \tag{4-27}$$

where S_f is the surface area occupied by one mole of interfacial atoms. S_f is therefore expressed as $S_f = \alpha_A S_{fA} + \alpha_B S_{fB}$, in which α_A and α_B are the fractions of interfacial atoms A and B, respectively, versus the total atoms in shell−core structures. Here, $\alpha_A = x_A(h_A)/(L_A)$ and $\alpha_B = x_B(h_B)/(L_B)$ where L_A and L_B are the thickness of original interface layer and x is the atomic concentration.

5.4. Kinetic Considerations

Since the thermodynamic driving force in a shell−core structure with miscible bimetallic elements creates the possibility of interfacial alloying, the kinetic approach seems essential to describe the alloying.[213] In this section, we propose the diffusion kinetics for interfacial alloying in a shell−core nanoparticle, as shown in Figure 20.

The size-dependent amplitude $\sigma(r)$ of the atomic thermal vibration of nanocrystals is as follows[214]

$$\sigma^2(r)/\sigma_\infty{}^2 = \exp[(\alpha - 1)x] = \exp[(\phi - 1)n_s/n_\upsilon] \tag{4-28}$$

where r is the radius of nanocrystals, the subscripts s and υ denote the surface and interior values of the number of atoms n and the atomic vibration amplitude σ, $\sigma_\infty{}^2$ is the mean-square displacement (msd) for the corresponding bulk crystal, ϕ is the ratio of σ_s/σ_υ, and $x = n_s/n_\upsilon$. For components A and B, the ratio of the number of atoms in the interface and interior are obtained, respectively, as

$$x_A = n_{s_A}/n_{\upsilon_A} = \frac{4\pi r^2 h_A/V_{0A}}{\frac{4}{3}\pi r^3/V_{0A} - 4\pi r^2 h_A/V_{0A}} = \frac{3h_A}{r - 3h_A} \tag{4-29}$$

$$x_B = n_{s_B}/n_{\upsilon_B} = \frac{4\pi r_A^2 h_B/V_{0B}}{\left(\frac{4}{3}\pi r^3 - \frac{4}{3}\pi r_A^3\right)/V_{0B} - 4\pi r_A^2 h_B/V_{0B}} = \frac{3 r_A^2 h_B}{(r^3 - r_A^3) - 3r_A^2 h_B} \tag{4-30}$$

When the shape of the shell−core nanoparticle is taken to be a sphere or quasi-sphere, V_0 and h state the volume of nanoparticles and the atomic diameter, respectively. Note that the r must be for more than one monolayer of atoms to guarantee a bimetallic interface. Under the high-temperature approximation,[214] $\sigma^2(r)/\sigma^2_\infty = T_m(\infty)/T_m(r)$, in which $T_m(\infty)$ and $T_m(r)$ denote the bulk and the size-dependent melting temperature, respectively. According to the Boltzmann−Arrhenius dependence of the diffusion coefficient D_{iff} on temperature[202]

$$D_{iff} = D_{iff_0}\exp(-E_{diff}/RT) \tag{4-31}$$

where E_{diff}, R, and T are the diffusion activation energy, the ideal gas constant, and the absolute temperature, respectively. Note that many researchers have reported for the size-dependence of the melting temperature of free nanoparticles[202] that the melting temperature decreases with reduction of size. Dick et al.[202] studied the size-dependent melting temperature of gold particles and assumed the diffusion coefficients at the melting point are the same and are independent of the melting temperature and size, i.e., $D_{iff}[r,T_m(r)] = D_{iff}[r(\infty),T_m(\infty)]$. Furthermore, based on the point defect mechanism,[215] the diffusion coefficient in a cubic crystal can be written as

$$D_{iff} = D_{iff_0}\exp(-\Delta H_m/(RT)) \tag{4-32a}$$

with

$$D_{iff0} = \frac{1}{6}a^2 z P_V \nu \exp(\Delta S_m/R) \tag{4-32b}$$

where D_{iff_0} represents the pre-exponential factor. a, z, P_V, υ, ΔS_m, and ΔH_m are the unit movement distance for an atom, the coordinate numbers, the probability of vacancy in a neighboring position, the vibration frequency of the atoms, the activation entropy, and the activation enthalpy, respectively. However, the vibration frequency shift is about 1%−5% even in the large scale of 2−50 nm.[216] Thus, the change of ΔS_m originating from the vibrational frequency change in the activation process is very small. Thus, we conclude that D_{iff_0} is only a weak function of the particle size and can, as an approximation, take $D_{iff_0}$to be constant. We deduce the relationship between the diffusion activation energy and the temperature to be $E_{diff}(r)/E_{diff}(\infty) = T_m(r)/T_m(\infty)$.

Therefore, $\sigma^2(r)/\sigma^2_\infty = T_m(\infty)/T_m(r) = \exp[(1 - \phi)x]$. On the basis of the vibration entropy expression of Mott, ϕ can be expressed as $\phi = [2S_\infty/3R + 1]$,[212] in which S_∞ is the bulk melting entropy. Accordingly, $E_{diff}(r) = E(\infty)\exp(-2S_\infty/(3R)x)$.

From the above, it follows that the size-dependent diffusion coefficients with A in B and B in A are, respectively,

$$D_{iff_{B\to A}}(r,T) = D_{iff_{A0}}\exp\left[\frac{-E_{diff_A}(\infty)}{RT}\exp\left[\frac{-2S_{A\infty}}{3R}\times\frac{3h_A}{r-3h_A}\right]\right] \tag{4-33}$$

$$D_{iff_{A\to B}}(r,T) = D_{iff_{B0}}\exp\left[\frac{-E_{diff_B}(\infty)}{RT}\exp\left[\frac{-2S_{B\infty}}{3R}\times\frac{3r_A^2h_B}{(r^3-r_A^3)-3r_A^2h_B}\right]\right] \tag{4-34}$$

According to Darken's equation, i.e., $D_{diff}\tilde{} = C_A D_{diff_B} + C_B D_{diff_A}$,[217] the $D\tilde{}_{diff}$, D_{iff_i} (i = A, B), and C_j (j = A, B) denote the interdiffusion coefficient, the partial-diffusion coefficient, and the fractional concentration, respectively, with $C_A + C_B = 1$. In this approach, $D_{iff_{B\to A}}(r,T)$ and $D_{iff_{A\to B}}(r,T)$ are written as the partial-diffusion coefficient with D_{iff_B} and D_{iff_A}.

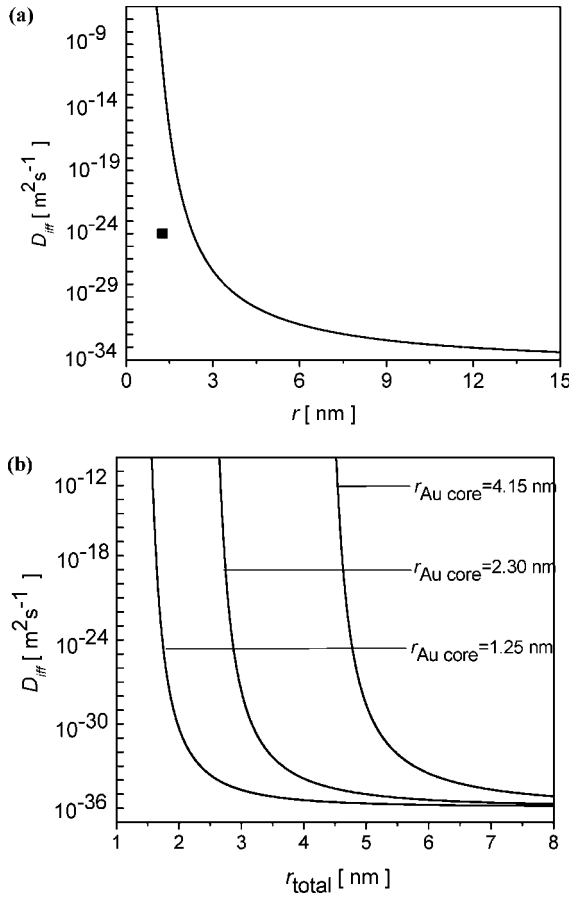

Figure 21. Size-dependent diffusion coefficient D at normal temperature of 300 K, (a) for Ag atom diffusion into Au core and parameters for Ag diffusion into Au core are listed as following: $D_0 = 7.2E - 6$ m^2 s^{-1}, and $E(\infty) = 169.8$ kJ mol^{-1}.[221] (b) For Au atom diffusion into Ag shell at different diameters of A, B and C with 2.5, 4.6, and 8.3 nm, respectively. The symbol (■) with the corresponding size denotes the experimental results where $D(1.25, 300\ K) = 1.0E - 24$ m^2 s^{-1}.[28] Some parameters for Au atom diffusion into Ag shell are as follows: $D_0 = 4E - 6$ m^2 s^{-1}, $E(\infty) = 169.5$ kJ mol^{-1}, and $T = 300$ K, respectively;[221] others are listed in Table 1.

Equations 4-33 and 4-34 correspond to the B shell diffusion into the A core and vice versa, respectively.

5.5. Au/Ag Bimetallic System

The typical Au−Ag nanoparticle having an Au core and an Ag shell is taken as an example to check the validity of the proposed theory. According to eq 4-27, we can conclude that the thermodynamic driving force is size-dependent, and the size of the shell−core structure can greatly influence the value of the driving force at the nanometer scale. We note that the heat of formation in miscible bimetallic systems is negative so that the driving force can be larger than zero. Accordingly, the interface of the Au−Ag shell−core structure generates a huge thermodynamic driving force to drive interface alloying at ambient temperature. These results show that, for the Au−Ag nanoparticle under normal conditions, spontaneous interface alloying seems thermodynamically possible because of the large thermodynamic driving force of the system. In fact, the experiments of Meisel and coworkers[28] have substantiated the theoretical prediction above.

In Figure 21, we plot the size-dependent diffusion coefficient according to eqs 4-33 and 4-34, which lead to the anomalous diffusion near the interface in the shell−core structure. The relevant parameters used in our calculations are listed in Table 1. From Figure 21a, we can see that the diffusion coefficient of Ag into Au smoothly decreases with increasing radius of the Au core and finally goes to the bulk diffusion coefficient. However, we definitely see that there exists a threshold value of the diffusion coefficient at a core radius of about 2.5 nm. In detail, the diffusion coefficient rapidly increases with decreasing radius of the Au core and goes to an unconventionally high value when the radius is less than 2.5 nm. For example, when the radius of the core is about 2 nm, the diffusion coefficient reaches 10^{-24} m^2 s^{-1}, which is consistent with the experiment.[28]

From the above results, the diffusion of shell into core depends on the size of the core to a certain extent. Thus, the smaller the radius of the core, the more intense is the interfacial diffusion, which corresponds to the experimental observations.[28,204] Similarly, for the case of the diffusion of Au core into Ag shell, the diffusion coefficient is shown in Figure 21b. Diffusion behaviors are shown when the radius of the Au core is 2.5, 4.6, and 8.3 nm. Note that when the Ag shell is very thin, the diffusion coefficient of Au core into Ag shell quickly increases with decreasing thickness of the Ag shell and decreases with increasing the thickness of the shell. Very importantly, the experimental data strongly supports these theoretical predictions.[28] For example, for a nanoparticle of 2 nm radius at room temperature, the diffusion coefficient of Au is calculated to be 10^{-28} m^2 s^{-1}, which is in good agreement with the experimental data.[28,202] However, the corresponding bulk diffusion coefficient is just 10^{-36} m^2 s^{-1}. Apparently the kinetics of the unusually high diffusion coefficient at the nanometer scale corresponds to the ambient temperature, size-dependent spontaneous interfacial alloying in the Au−Ag nanoparticle. Furthermore, the three curves in Figure 21b have homologous character, suggesting that both the core-into-shell and shell-into-core diffusion behavior are actually size-dependent at the nanometer scale. As the size of both the core and the shell increase, the diffusion coefficient decreases, and the corresponding diffusion concentration is very low, while at small sizes of the core/shell structure, the diffusion is facile because of the effects at the nanometer scale.

Predictions from the above theory treating these physical and chemical processes that have fast spontaneous intermixing in binary metallic nanoparticles are in good agreement with previous experimental studies[28,218] and atomistic simulations.[219,220] Thus, nanometer-scale, size-dependent diffusion provides a clear example of ambient temperature interfacial alloying in the shell−core. Naturally, the rate of the interfacial alloying depends on both the size of the core and the total size of the shell−core nanoparticles. Overall, the above thermodynamic and kinetic approaches to size-dependent spontaneous interfacial alloying in a shell−core structure perform well in the case of Au−Ag nanoparticles, thus implying that this is a general theory for interfacial behavior in shell−core nanostructures.

5.6. Summary

We have treated the size dependent spontaneous interfacial alloying in metallic shell−core nanoparticles under the assumption of the correlation of the size-dependent surface energy to the heat of formation. For miscible bimetallic systems, the large thermodynamic driving force from the size-dependent negative mixing enthalpy and the shell−core interface energy creates the possibility for an ambient

Table 1. Numerical Parameters Used in the Text;[50,101,222] Note That the S_{vib} Means the Vibration Entropy for Si

	h (nm)	S_{mb} (J mol^{-1} K^{-1})	H_{mb} (kJ mol^{-1})	V_s (cm^3 mol^{-1})	k ($\times 10^{-12}$ (Pa^{-1})	E_0 (GPa)	ν	γ_0 (J m^{-2})
Ag	0.2889	9.16	11.3	10.3	9.6225	83		1.25
Au	0.2884	9.38	12.55	10.2	5.848	78	0.44	1.59
Si	0.1568	6.7 (S_{vib})	50.55	15.7	0.306	47		1.24
Cu	0.2556	9.65	13.1	7.11		130	0.34	1.592

temperature spontaneous alloying arising from the interface in a shell−core nanoparticle. These results thus suggest that the thermodynamic origins correspond to the anomalous alloying. Meanwhile, the unusually high ambient temperature diffusion coefficient between the core and shell near the interface provides a kinetic route to achieve the interfacial alloying, which is apparently the kinetic mechanism for the process. Interestingly, the agreement between the theoretical predictions and the experimental data implies that the model established here can be expected to be a universal approach to interfacial behavior in shell−core nanostructures.

6. Concluding Remarks

We have shown that the effect of the negative curvature of nanostructures has enabled us to view the performance of a surface or interface from the perspective of both nanometer-scale thermodynamics and continuum mechanics. The progress made can be summarized as follows:

(i) The unusual state of atoms at the inner skin of nanocavities has been related to the size dependence of the surface energy. Three components of nanocavities (the liquid-like matrix, the vapor-like cavity, and the inner surface skin of the cavity) have been considered in the cavity-matrix structure, and surface energy contributions from chemical and structural effects have been discussed. It has been found that the surface energy increases with the inverse of the cavity size and that the cavity shrinks in size, which are different from what we would usually expect. It is suggested that the surface skin will be stronger than that of the matrix because of the bond-order deficiency effect.

(ii) The action of nanocavities in host crystals as a sink for metallic impurity atoms is proposed on the basis of the thermodynamic and kinetic approaches applied at the nanometer scale. The impurity trapping mechanisms of nanocavities are attributed in the thermodynamic approach to the contact epitaxy of impurity atoms on the inner surface of nanocavities and, in the kinetic approach, to the diffusion flux of impurity atoms being oriented toward nanocavities in host crystals. These theoretical results demonstrate that the nanocavities in host crystals could be used as a functional unit to fabricate nanodevices. Furthermore, melting behaviors of nanocavities in a matrix have been investigated on the basis of both nanometer-scale thermodynamics and continuum medium mechanics. An analytical model was established to elucidate the kinetics of nanocavity shrinkage under external thermal activation and the melting thermodynamics of nanocavities. It was found that the shrinkage of a nanocavity exhibits a pronounced nonlinear kinetic character as the size of the nanocavity size progresses through several nanometer scales. Additionally, a huge superheating of a nanocavity of small size appears when the temperature is equal to the melting point of the matrix. The size-dependent inner surface energy of the nanocavity is apparently responsible for these anomalous melting behaviors.

(iii) An analytic theory has been developed from the perspective of thermodynamics and continuum medium mechanics to predict and explain the mechanical responses of nanotubes as their structure changes. It was found that the surface energy of the inner surface increases while the surface energy of the outer surface decreases with decreasing diameter of the nanotubes, thus leading to the anomalous increase of Young's modulus of a nanotube as its diameter decreases. For the same material, the Young's modulus of a nanotube with a thin shell is higher than that of one with a thick shell, and the Young's modulus of a nanotube is higher than that of a nanowire with the same size. The Young's modulus of both a nanotube and a nanowire are larger than that of the bulk material. Importantly, theoretical predictions are consistent with experiments. Moreover, we established an analytic theory to predict the mechanical responses of nanoporous structures from the perspective of nanothermodynamics and continuum mechanics and showed that the effective bulk elastic modulus of nanoporous structures with pore size less than 2 nm is larger than that of the bulk counterpart. It was found that the inner surface stiffening induced by the size-dependent inner surface energy of cylindrical nanopores appears to be the physical origin of the anomalous mechanical properties of nanoporous structures. The agreement between theory and experiment suggests that the proposed theory could be expected to be applicable to nanoporous structural materials.

(iv) The size-dependent thermodynamic and kinetic models were derived to elucidate the physical and chemical origins of the thermodynamic driving force causing the spontaneous interfacial alloying and the anomalous diffusion arising from the metallic shell−core interface in nanoparticles. It was found that, in the thermodynamic view, the very large driving force arising from the size-dependent mixing enthalpy and the interfacial energy leads to spontaneous interfacial alloying. In the kinetic view, the unusually intense interfacial diffusion provides a path to achieve ambient temperature interfacial alloying. Interestingly, these theoretical predictions are in agreement with the experimental data.

It should be emphasized that all the theoretical models mentioned above are successful from different aspects such as mechanics, nucleation and interfacial alloying, etc., and with the size-dependent surface energy of negative curvature nanostructures as the complementary origin, they would be complete and in good accordance. On the other hand, considering that almost all of the physical properties of nanomaterials are consistently related to the surface or interface free energy, the significance of these theoretical approaches is that, with only a few adjustable parameters, they successfully treat the whole range from zero-dimensional to one-dimensional, two-dimensional, and three-dimensional nanostructures. More strikingly, as the current theoretical methods are the first-order approximation, there is still plenty of room for improvement by involving other external stimuli such as temperature, pressure, and electrical or magnetic field approaches that contribute to the surface state of negative curvature nanostructures. Thus, it is really an open topic full of exciting challenges. Further investigation should be pursued in the near future.

7. Acknowledgments

This work was financially supported by the National Natural Science Foundation of China (Grant Nos. 10804030, 50525206, and U0734004), the Ministry of Education (106126, 209088), and the Scientific Research Fund of Hunan Provincial Education Department (08B052).

8. References

(1) Yasuda, H.; Tanaka, A.; Matsumoto, K.; Nitta, N.; Mori, H. *Phys. Rev. Lett.* **2008**, *100*, 105506.
(2) Dil, H.; Lobo-Checa, J.; Laskowski, R.; Blaha, P.; Berner, S.; Osterwalder, J.; Greber, T. *Science* **2008**, *319*, 1824.
(3) Mercier, L.; Pinnavaia, T. J. *Adv. Mater.* **1997**, *9*, 500.
(4) De Vos, D. E.; Dams, M.; Sels, B. F.; Jacobs, P. A. *Chem. Rev.* **2002**, *102*, 3615.
(5) Sen, T.; Sebastianelli, A.; Bruce, L. J. *J. Am. Chem. Soc.* **2006**, *128*, 7130.
(6) Yu, C. C.; Zhang, L. X.; Shi, J. L.; Zhao, J. J.; Gao, J. H.; Yan, D. S. *Adv. Funct. Mater.* **2008**, *18*, 1.
(7) Mohadjeri, B.; Williams, J. S.; Wong-Leung, J. *Appl. Phys. Lett.* **1995**, *66*, 1889.
(8) Wong-Leung, J.; Ascheron, C. E.; Petravic, M.; Elliman, R. G.; Williams, J. S. *Appl. Phys. Lett.* **1995**, *66*, 1231.
(9) Yang, G. W.; Liu, B. X. *Phys. Rev. B* **2000**, *61*, 4500.
(10) Wang, C. X.; Yang, G. W. *Mater. Sci. Eng., R* **2005**, *49*, 157.
(11) Sun, C. Q. *Prog. Mater. Sci.* **2009**, *54*, 179.
(12) Ouyang, G.; Tan, X.; Yang, G. W. *Phys. Rev. B* **2006**, *74*, 195408.
(13) Ouyang, G.; Tan, X.; Cai, M. Q.; Yang, G. W. *Appl. Phys. Lett.* **2006**, *89*, 183104.
(14) Caruso, F.; Caruso, R. A.; Mohwald, H. *Science* **1998**, *282*, 1111.
(15) Sun, Y. G.; Xia, Y. N. *Science* **2002**, *298*, 2176.
(16) Zeng, H. B.; Cai, W. P.; Liu, P. S.; Xu, X. X.; Zhou, H. J.; Klingshirn, C.; Kalt, H. *ACS Nano* **2008**, *2*, 1661.
(17) Chen, Z. T.; Gao, L. *Cryst. Growth Des.* **2008**, *8*, 460.
(18) Li, Z. Q.; Xie, Y.; Xiong, Y. J.; Zhang, R. *New J. Chem.* **2003**, *27*, 1518.
(19) Tu, K. N.; Gösele, U. *Appl. Phys. Lett.* **2005**, *86*, 093111.
(20) Huang, W. J.; Sun, R.; Tao, J.; Menard, L. D.; Nuzzo, R. G.; Zuo, J. M. *Nat. Mater.* **2008**, *7*, 308.
(21) Mironets, O.; Meyerheim, H. L.; Tusche, C.; Stepanyuk, V. S.; Soyka, E.; Zschack, P.; Hong, H.; Jeutter, N.; Felici, R.; Kirschner, J. *Phys. Rev. Lett.* **2008**, *100*, 096103.
(22) Needs, R. J. *Phys. Rev. Lett.* **1987**, *58*, 53.
(23) Fischer, F. D.; Waitz, T.; Vollath, D.; Simha, N. K. *Prog. Mater. Sci.* **2008**, *53*, 481.
(24) Nanda, K. K.; Kruis, F. E.; Fissan, H. *Phys. Rev. Lett.* **2002**, *89*, 256103.
(25) Nanda, K. K.; Maisels, A.; Kruis, F. E.; Fissan, H.; Stappert, S. *Phys. Rev. Lett.* **2003**, *91*, 106102.
(26) Ouyang, G.; Tan, X.; Wang, C. X.; Yang, G. W. *Nanotechnology* **2006**, *17*, 4257.
(27) Giorgio, S.; Henry, C. R. *Eur. Phys. J. Appl. Phys.* **2002**, *20*, 23.
(28) Shibata, T.; Bunker, B. A.; Zhang, Z.; Meisel, D. *J. Am. Chem. Soc.* **2002**, *124*, 11989.
(29) Loufova, S. S.; Vlckova, B.; Bastls, Z.; Hasslett, T. L. *Langmuir* **2004**, *20*, 3407.
(30) Selvakannan, P. R.; Swami, A.; Srisathiyanarayanan, D.; Shirude, P. S.; Pasricha, R.; Mandale, A. B.; Sastry, M. *Langmuir* **2004**, *20*, 7825.
(31) Damle, C.; Biswas, K.; Sastry, M. *Langmuir* **2001**, *17*, 7156.
(32) Doudna, C. M.; Bertino, M. F.; Blum, F. D.; Tokuhiro, A. T.; L-Dey, D.; Chattopadhyay, S.; Terry, J. *J. Phys. Chem. B* **2003**, *107*, 2966.
(33) Still, T.; Sainidou, R.; Retsch, M.; Jonas, U.; Spahn, P.; Hellmann, G. P.; Fytas, G. *Nano Lett.* **2008**, *8*, 3194.
(34) Férey, G.; Mellot-Draznieks, C.; Sere, C.; Millange, F.; Dutour, J.; Surblé, S.; Margiolaki, I. *Science* **2005**, *309*, 2040.
(35) Li, R.; Sieradzki, K. *Phys. Rev. Lett.* **1992**, *68*, 1168.
(36) Biener, J.; Hodge, A. M.; Hayes, J. R.; Volkert, C. A.; Zepeda-Ruiz, L. A.; Hamza, A. V.; Abraham, F. F. *Nano Lett.* **2006**, *6*, 2379.
(37) Mathur, A.; Erlebacher, J. *Appl. Phys. Lett.* **2007**, *90*, 061910.
(38) Rowsell, J. L. C.; Millward, A. R.; Park, K. S.; Yaghi, O. M. *J. Am. Chem. Soc.* **2004**, *126*, 5666.
(39) Lee, J. H.; Galli, G. A.; Grossman, J. C. *Nano Lett.* **2008**, *8*, 3750.
(40) Zhu, X. F. *J. Appl. Phys.* **2006**, *100*, 034304.
(41) Smmalkorpi, M.; Krasheninnikov, A.; Kuronen, A.; Nordlund, K.; Kaski, K. *Phys. Rev. B* **2004**, *70*, 245416.
(42) Wong, E. W.; Sheehan, P. E.; Lieber, C. M. *Science* **1997**, *277*, 1971.
(43) Ren, Y.; Fu, Y. Q.; Liao, K.; Li, F.; Cheng, H. M. *Appl. Phys. Lett.* **2004**, *84*, 2811.
(44) Tu, Z. C.; Ouyang, Z. C. *Phys. Rev. B* **2002**, *65*, 233407.
(45) Feng, X. Q.; Xia, R.; Li, X. D.; Li, B. *Appl. Phys. Lett.* **2009**, *94*, 0119216.
(46) Adamson, A. W. *Physical chemistry of surfaces*; John Wily & Sons, Inc.: New York, 1990.
(47) Shuttleworth, R. *Proc. Phys. Soc. A (London)* **1950**, *63*, 444.
(48) Naher, U.; Bjrnholm, S.; Frauendorf, S.; Garcias, F.; Guet, C. *Phys. Rep.* **1997**, *285*, 245.
(49) Brechignac, C.; Busch, H.; Cahuzac, Ph.; Leygnier, J. *J. Chem. Phys.* **1994**, *101*, 6992.
(50) Nanda, K. K.; Sahu, S. N.; Behera, S. N. *Phys. Rev. A* **2002**, *66*, 0132208.
(51) Rose, J. H.; Vary, J. P.; Smith, J. R. *Phys. Rev. Lett.* **1984**, *53*, 344.
(52) Rose, J. H.; Smith, J. R.; Ferrante, J. *Phys. Rev. B* **1983**, *28*, 1835.
(53) Tomanek, D.; Mukherjee, S.; Bennemann, K. H. *Phys. Rev. B* **1983**, *28*, 665.
(54) Vanithakumari, S. C.; Nanda, K. K. *Phys. Lett. A* **2008**, *372*, 6930.
(55) Sun, C. Q.; Tay, B. K.; Lau, S. P.; Sun, X.; Zeng, X. T.; Bai, H. L.; Liu, H.; Liu, Z. H.; Jiang, E. Y. *J. Appl. Phys.* **2001**, *90*, 2615.
(56) Seifert, G.; Vietze, K.; Schmidt, R. *J. Phys. B* **1996**, *29*, 5183.
(57) Sun, C. Q. *Prog. Solid State Chem.* **2007**, *35*, 1.
(58) Goldschmidt, V. M. *Ber. Deut. Chem. Ges.* **1927**, *60*, 1270.
(59) Pauling, L. *J. Am. Chem. Soc.* **1947**, *69*, 542.
(60) Feibelman, P. J. *Phys. Rev. B* **1996**, *53*, 13740.
(61) Ouyang, G.; Gu, M. X.; Fu, S. Y.; Sun, C. Q.; Zhu, W. G. *Europhys. Lett.* **2008**, *84*, 660005.
(62) Ouyang, G.; Li, X. L.; Yang, G. W. *Appl. Phys. Lett.* **2007**, *91*, 051901.
(63) Ouyang, G.; Li, X. L.; Tan, X.; Yang, G. W. *Nanotechnology* **2008**, *19*, 045709.
(64) Hill, T. L. *Thermodynamics of Small Systems*, Vol. I; W. A. Benjamin: New York, 1963.
(65) Hill, T. L. *Thermodynamics of Small Systems*, Vol. II; W. A. Benjamin: New York, 1964.
(66) Hill, T. L. *J. Chem. Phys.* **1962**, *36*, 3182.
(67) Hill, T. L. *J. Chem. Phys.* **1961**, *34*, 1974.
(68) Hill, T. L. *J. Chem. Phys.* **1961**, *35*, 303.
(69) Hill, T. L. *Proc. Natl. Acad. Sci. U.S.A.* **1996**, *93*, 14328.
(70) Hill, T. L.; Chamberlin, R. V. *Proc. Natl. Acad. Sci. U.S.A.* **1998**, *95*, 12779.
(71) Hill, T. L. *Nano Lett.* **2001**, *1*, 273.
(72) Hill, T. L. *Nano Lett.* **2001**, *1*, 159.
(73) Hill, T. L. *Nano. Lett.* **2001**, *1*, 111.
(74) Hill, T. L.; Chamberlin, R. V. *Nano Lett.* **2002**, *2*, 609.
(75) Chamberlin, R. V. *Phys. Rev. Lett.* **1999**, *82*, 2520.
(76) Chamberlin, R. V. *Phase Transitions* **1999**, *65*, 169.
(77) Chamberlin, R. V. *Phys. Rev. Lett.* **1999**, *83*, 5134.
(78) Chamberlin, R. V. *Nature* **2000**, *408*, 337.
(79) Chamberlin, R. V. *Phys. Rev. Lett.* **2001**, *87*, 129601.
(80) Chamberlin, R. V.; Humfeld, K. D.; Farrell, D.; Yamamuro, S.; Ijiri, Y.; Majetich, S. A. *J. Appl. Phys.* **2002**, *91*, 6961.
(81) Chamberlin, R. V. *Science* **2002**, *298*, 1172.
(82) Chamberlin, R. V.; Hemberger, J.; Loidl, A.; Humfeld, K. D.; Farrell, D.; Yamamuro, S.; Ijiri, Y.; Majetich, S. A. *Phys. Rev. B* **2002**, *66*, 172403.
(83) Chamberlin, R. V. *Phys. Lett. A* **2003**, *315*, 313.
(84) Chamberlin, R. V. *ACS Symp. Ser.* **2002**, *820*, 228.
(85) Fahey, P. M.; Griffin, P. B.; Plummer, J. D. *Rev. Mod. Phys.* **1989**, *61*, 289.
(86) Kyllesbech Larsen, K.; Privitera, V.; Coffa, S.; Priolo, F.; Campisano, S. U.; Carnera, A. *Phys. Rev. Lett.* **1996**, *76*, 1493.
(87) Coyle, S.; Netti, M. C.; Baumberg, J. J.; Ghanem, M. A.; Birkin, P. R.; Bartlett, P. N.; Whittaker, D. M. *Phys. Rev. Lett.* **2001**, *87*, 176801.
(88) Gu, L.; Cheley, S.; Bayley, H. *Science* **2001**, *291*, 636.
(89) Ruault, M. O.; Fortuna, F.; Bernas, H.; Ridgway, M. C.; Willams, J. S. *Appl. Phys. Lett.* **2002**, *81*, 2617.
(90) Brusa, R. S.; Macchi, C.; Mariazzi, S.; Karwasz, G. P.; Egger, W.; Sperr, P.; Kögel, G. *Phys. Rev. B* **2005**, *71*, 245320.
(91) Seager, C. H.; Myers, S. M.; Anderson, R. A.; Warren, W. L.; Follstaedt, D. M. *Phys. Rev. B* **1994**, *50*, 2458.
(92) Rest, J.; Birtcher, R. C. *J. Nucl. Mater.* **1989**, *168*, 312.
(93) Wang, L. M.; Birtcher, R. C. *Appl. Phys. Lett.* **1989**, *55*, 2494.
(94) Kim, J. C.; Cahill, D. G.; Averback, R. S. *Phys. Rev. B* **2003**, *68*, 094109.
(95) Ishikawa, N.; Awaji, M.; Furuya, K.; Birtcher, R. C.; Allen, C. W. *Nucl. Instrum. Methods Phys. Res., Sect. B* **1997**, *127−128*, 123.
(96) Zhu, X. F. *J. Phys: Condens. Matter* **2003**, *15*, L253.
(97) Williams, J. S.; Zhu, X. F.; Ridgway, M. C.; Conway, M. J.; Williams, B. C.; Fortuna, F.; Ruault, M. O.; Bernas, H. *Appl. Phys. Lett.* **2000**, *77*, 4280.
(98) Zhu, X. F.; Williams, J. S.; Conway, M. J.; Ridgway, M. C.; Fortuna, F.; Ruault, M. O.; Bernas, H. *Appl. Phys. Lett.* **2001**, *79*, 3416.

(99) Moody, M. P.; Attard, P. *Phys. Rev. Lett.* **2003**, *91*, 056104.
(100) Ouyang, G.; Liang, L. H.; Wang, C. X.; Yang, G. W. *Appl. Phys. Lett.* **2006**, *88*, 091914.
(101) Dingrevillea, R.; Qu, J. M.; Cherkaoui, M. *J. Mech. Phys. Solids* **2005**, *53*, 1827.
(102) Fried, E.; Gurtin, M. E. In *Advances in Applied Mechanics*, Vol. 40; Aref, H., Van der Giessen, E., Eds.; Academic Press: Salt Lake City, UT, 2004; pp 1−177.
(103) Sun, C. Q.; Shi, Y.; Li, C. M.; Li, S.; Au Yeung, T. C. *Phys. Rev. B* **2006**, *73*, 075408.
(104) Lu, H. M.; Jiang, Q. *J. Phys. Chem. B* **2004**, *108*, 5617.
(105) Buff, F. R. *J. Chem. Phys.* **1951**, *19*, 1591.
(106) Tolman, R. C. *J. Chem. Phys.* **1949**, *17*, 333.
(107) Koenig, F. O. *J. Chem. Phys.* **1950**, *18*, 449.
(108) Kirkwood, J. G.; Buff, F. P. *J. Chem. Phys.* **1949**, *17*, 338.
(109) Nijmeijer, M. J. P.; Bruin, C.; van Woerkom, A. B.; Bakker, A. F. *J. Chem. Phys.* **1992**, *96*, 565.
(110) Moody, M. P.; Attard, P. *J. Chem. Phys.* **2001**, *115*, 8967.
(111) Saito, Y.; Uemura, H.; Uwaha, M. *Phys. Rev. B* **2001**, *63*, 045422.
(112) Weissmuller, J.; Cahn, J. W. *Acta Mater.* **1997**, *45*, 1899.
(113) Lamber, R.; Werjen, S.; Jaeger, N. I. *Phys. Rev. B* **1998**, *51*, 10968.
(114) Liang, L. H.; Li, J. C.; Jiang, Q. *Physica B* **2003**, *334*, 49.
(115) Chaudhari, P.; Spaepen, F.; Steinhardt, P. J. *Glass Metals II*; Beck, H., Güntherodt, H.-J., Eds.; Springer: Berlin, 1983; Chapter 5.
(116) Yang, F. Q. *J. Appl. Phys.* **2004**, *95*, 3516.
(117) Brett, D. A.; Llewellyn, D. J.; Ridgway, M. C. *Appl. Phys. Lett.* **2006**, *88*, 222107.
(118) Ruault, M. O.; Ridgway, M. C.; Fortuna, F.; Bernas, H.; Williams, J. S. *Eur. Phys. J: Appl. Phys.* **2003**, *23*, 39.
(119) Bai, B. M.; Li, M. *Nano Lett.* **2006**, *6*, 2284.
(120) Goldstein, A. N.; Echer, C. M.; Alivisatos, A. P. *Science* **1992**, *256*, 1425.
(121) Ouyang, G.; Li, X. L.; Tan, X.; Yang, G. W. *Appl. Phys. Lett.* **2006**, *89*, 031904.
(122) Ren, F.; Jiang, G. Z.; Liu, C.; Wang, J. B. *Phys. Rev. Lett.* **2006**, *97*, 165501.
(123) Eaglesham, D. J.; White, A. E.; Feldman, L. C.; Moriya, N.; Jacobson, D. C. *Phys. Rev. Lett.* **1993**, *70*, 1643.
(124) Cerofolini, G. F.; Corni, F.; Frabboni, S.; Nobili, C.; Ottaviani, G.; Tonini, R. *Mater. Sci. Eng., R* **2000**, *27*, 1.
(125) Brooks, H. *Impurities and Imperfection*; American Society for Metals: Cleveland, OH, 1955.
(126) Qi, W. H.; Wang, M. P. *Physica B* **2003**, *334*, 432.
(127) Zhu, X. F.; Wang, Z. G. *Chin. Phys. Lett.* **2005**, *22*, 657.
(128) Kovač, D.; Otto, G.; Hobler, G. *Nucl. Instrum. Methods Phys. Res., Sect. B* **2005**, *228*, 226.
(129) Ruault, M. O.; Ridgway, M. C.; Fortuna, F.; Bernas, H.; Williams, J. S. *Nucl. Instrum. Methods B* **2003**, *206*, 912.
(130) Schmidt, H.; Borchardt, G.; Rudolphi, M.; Baumann, H.; Bruns, M. *Appl. Phys. Lett.* **2004**, *85*, 582.
(131) Schmidt, H.; Gupta, M.; Bruns, M. *Phys. Rev. Lett.* **2006**, *96*, 055901.
(132) Altug, H.; Englund, D.; Vuckovic, J. *Nature Phys.* **2006**, *2*, 484.
(133) Périchaud, I.; Yakimov, E.; Martinuzzi, S.; Dubois, C. *J. Appl. Phys.* **2001**, *90*, 2806.
(134) Brett, D. A.; de M. Azevedo, G.; Llewellyn, D. J.; Ridgway, M. C. *Appl. Phys. Lett.* **2003**, *83*, 946.
(135) Raineri, V.; Fallica, P. G.; Percolla, G.; Bataglia, A.; Barbagallo, M; Campisano, S. U. *J. Appl. Phys.* **1995**, *78*, 3727.
(136) Myers, S. M.; Petersen, G. A.; Seager, C. H. *J. Appl. Phys.* **1996**, *80*, 3717.
(137) Roqueta, F.; Ventura, L.; Grob, J. J.; Jérisian, R. *J. Appl. Phys.* **2000**, *88*, 5000.
(138) Brett, D. A.; Llewellyn, D. J.; Ridgway, M. C. *Nucl. Instrum. Methods B* **2006**, *242*, 576.
(139) Ou, X.; Kögler, R.; Mücklich, A.; Skorupa, W.; Möller, W.; Wang, X.; Gerlach, J. W.; Rauschenbach, B. *Appl. Phys. Lett.* **2008**, *93*, 161907.
(140) Ogura, A. *Appl. Phys. Lett.* **2003**, *82*, 4480.
(141) Deweerd, W.; Barancira, T.; Langouche, G.; Milants, K.; Moons, R.; Verheyden, J.; Pattyn, H. *Nucl. Instrum. Methods B* **1996**, *120*, 51.
(142) Kinomura, A.; Williams, J. S.; Wong-Leung, J.; Petravic, M. *Nucl. Instrum. Methods B* **1997**, *127−128*, 297.
(143) Ouyang, G.; Li, X. L.; Yang, G. W. *Appl. Phys. Lett.* **2008**, *92*, 051902.
(144) Volmer, M.; Weber, A. *Z. Phys. Chem.* **1925**, *119*, 277.
(145) Farkas, L. *Z. Phys. Chem.* **1927**, *125*, 236.
(146) Turnbull, D.; Fisher, J. C. *J. Chem. Phys.* **1949**, *17*, 71.
(147) Turnbull, D. *J. Chem. Phys.* **1950**, *18*, 198.
(148) Turnbull, D. *J. Chem. Phys.* **1952**, *20*, 411.
(149) Defay, R.; Prigogine, I. *Surface Tension and Adsorption*; Wiley: New York, 1951 (English translation, 1966).
(150) Pan, X. L.; Fan, Z. L.; Chen, W.; Ding, Y. J.; Luo, H. Y.; Bao, X. H. *Nat. Mater.* **2007**, *6*, 507.
(151) Xia, Y.; Yang, P.; Sun, Y.; Wu, Y.; Mayers, B.; Gates, B.; Yin, Y.; Kim, F.; Yan, H. *Adv. Mater.* **2003**, *15*, 353.
(152) Murray, C. B.; Kagan, C. R.; Bawendi, M. G. *Annu. Rev. Mater. Sci.* **2000**, *30*, 545.
(153) Li, R.; Luo, Z.; Papadimitrakopoulos, F. *J. Am. Chem. Soc.* **2006**, *128*, 6280.
(154) Chen, C. Q.; Shi, Y.; Zhang, Y. S.; Zhu, J.; Yan, Y. J. *Phys. Rev. Lett.* **2006**, *96*, 075505.
(155) Ouyang, G.; Yang, G. W.; Sun, C. Q.; Zhu, W. G. *Small* **2008**, *4*, 1359.
(156) Rodríguez, A. M.; Bozzolo, G.; Ferrante, J. *Surf. Sci.* **1993**, *289*, 100.
(157) Wang, B. L.; Yin, S. Y.; Wang, G. H.; Buldum, A.; Zhao, J. J. *Phys. Rev. Lett.* **2001**, *86*, 2046.
(158) Zhao, X. Y.; Wei, C. M.; Yang, L.; Chou, M. Y. *Phys. Rev. Lett.* **2004**, *92*, 236805.
(159) Sun, L.; Banhart, F.; Krasheninnikov, A. V.; Rodriguez-Manzo, J. A.; Terrones, M.; Ajayan, P. M. *Science* **2006**, *312*, 26.
(160) Robertson, D. H.; Brenner, D. W.; Mintmire, J. W. *Phys. Rev. B* **1992**, *45*, 12592.
(161) Yakobson, B. I.; Brabec, C. J.; Bernholc, J. *Phys. Rev. Lett.* **1996**, *76*, 2411.
(162) Lu, J. P. *Phys. Rev. Lett.* **1997**, *79*, 1297.
(163) Hernández, E.; Goze, C.; Bernier, P.; Rubio, A. *Phys. Rev. Lett.* **1998**, *80*, 4502.
(164) Cai, H.; Wang, X. *Nanotechnology* **2006**, *17*, 45.
(165) Hsieh, J.; Lu, J.; Huang, M.; Hwang, C. *Nanotechnology* **2006**, *17*, 3920.
(166) Treacy, M. M. J.; Ebbesen, T. W.; Gibson, J. M. *Nature* **1996**, *381*, 678.
(167) Poncharal, P.; Wang, Z. L.; Ugarte, D.; de Heer, W. A. *Science* **1999**, *283*, 1513.
(168) Chang, T.; Gao, H. *J. Mech. Phys. Solids* **2003**, *51*, 1059.
(169) Shen, L.; Li, J. *Phys. Rev. B* **2004**, *69*, 045414.
(170) Ouyang, G.; Li, X. L.; Tan, X.; Yang, G. W. *Phys. Rev. B* **2007**, *76*, 193406.
(171) Desjonqueres, M. C.; Spanjaard, D. In *Concepts in Surface Physics*; Springer Series in Surface Science, Vol. 30; Springer-Verlag: Berlin, Heidelberg, 1993.
(172) Galanakis, I.; Papanikolaou, N.; Dederichs, P. H. *Surf. Sci.* **2002**, *1*, 511.
(173) Kim, H. K.; Huh, S. H.; Park, J. W.; Jeong, J. W.; Lee, G. H. *Chem. Phys. Lett.* **2002**, *354*, 165.
(174) Sun, C. Q.; Wang, Y.; Tay, B. K.; Li, S.; Huang, H.; Zhang, Y. B. *J. Phys. Chem. B* **2002**, *106*, 10701.
(175) Jiang, Q.; Li, J. C.; Chi, B. Q. *Chem. Phys. Lett.* **2002**, *366*, 551.
(176) Sathyamoorthy, M. *Nonlinear Analysis of Structures*; CRC Press: Boca Raton, FL, 1998.
(177) Li, C.; Chou, T. W. *Phys. Rev. B* **2004**, *69*, 073401.
(178) Sun, C. Q. *Prog. Mater. Sci.* **2003**, *48*, 521.
(179) Gershow, M.; Golovchenko, J. A. *Nat. Nanotechnol.* **2007**, *2*, 775.
(180) Stein, D. *Nat. Nanotechnol.* **2007**, *2*, 741.
(181) Buyukserin, F.; Kang, M. C.; Martin, C. R. *Small* **2007**, *3*, 106.
(182) Uram, J. D.; Ke, K.; Hunt, A. J.; Mager, M. *Small* **2006**, *2*, 967.
(183) Lahav, M.; Sehayek, T.; Vaskevich, A.; Rubinstein, I. *Angew. Chem., Int. Ed. Engl.* **2003**, *42*, 5576.
(184) Chan, S.; Horner, S. R.; Fauchet, P. M.; Miller, B. L. *J. Am. Chem. Soc.* **2001**, *123*, 11797.
(185) Gaburro, Z.; Daldosso, N.; Pavesi, L.; Faglia, G.; Baratto, C.; Sberveglieri, G. *Appl. Phys. Lett.* **2001**, *78*, 3744.
(186) Ramakrishnan, N.; Arunachalam, V. S. *J. Am. Ceram. Soc.* **1993**, *76*, 2745.
(187) Munro, R. G. *J. Am. Ceram. Soc.* **2001**, *84*, 1190.
(188) Dean, E. A.; Lopez, J. A. *J. Am. Ceram. Soc.* **1983**, *66*, 366.
(189) Povstenko, Y. Z. *J. Mech. Phys. Solids* **1993**, *41*, 1499.
(190) Duan, H. L.; Wang, J.; Karihaloo, B. L.; Huang, Z. P. *Acta Mater.* **2006**, *54*, 2983.
(191) Sun, C. Q.; Tay, B. K.; Zeng, X. T.; Li, S.; Chen, T. P.; Zhou, J.; Bai, H. L.; Jiang, E. Y. *J. Phys.: Condens. Matter* **2002**, *14*, 7781.
(192) Wang, J.; Duan, H. L.; Zhang, Z.; Huang, Z. P. *Int. J. Mech. Sci.* **2005**, *47*, 701.
(193) Christensen, R. M.; Lo, K. H. *J. Mech. Phys. Solids* **1979**, *27*, 315.
(194) Kittel, C. *Introduction to Solid State Physics*, 6th ed.; Wiley: New York, 1986.
(195) Wu, X. F.; Dzenis, Y. A. *J. Appl. Phys.* **2007**, *102*, 044306.
(196) Chang, Y. A.; Pike, L. M.; Liu, C. T.; Bilbrey, A. R.; Stone, D. S. *Intermetallics* **1993**, *1*, 107.
(197) Yan, J.; Ma, X.; Zhao, W.; Tang, H.; Zhu, C.; Cai, S. *ChemPhysChem* **2005**, *6*, 2099.
(198) Biener, J.; Hodge, A. M.; Hamza, A. V.; Hsiung, L. M.; Satcher, J. H. *J. Appl. Phys.* **2005**, *97*, 024301.

(199) Parida, S.; Kramer, D.; Volckert, C. A.; Rosner, H.; Erlebacher, J.; Weissmuller, J. *Phys. Rev. Lett.* **2006**, *97*, 035504.
(200) Xia, Y.; Yang, P. *Adv. Mater.* **2003**, *15*, 351.
(201) Peters, K. F.; Cohen, J. B.; Chung, Y. W. *Phys. Rev. B* **1998**, *57*, 13430.
(202) Dick, K.; Dhanasekaran, T.; Zhang, Z. Y.; Meisel, D. *J. Am. Chem. Soc.* **2002**, *124*, 2312.
(203) Schware, R. B.; Johnson, W. L. *Phys. Rev. Lett.* **1983**, *51*, 415.
(204) Lin, C.; Yang, G. W.; Liu, B. X. *Phys. Rev. B* **2000**, *61*, 15649.
(205) Liu, B. X.; Lai, W. S.; Zhang, Z. *J. Adv. Phys.* **2001**, *50*, 367.
(206) Baletto, F.; Ferrando, R. *Rev. Mod. Phys.* **2005**, *77*, 371.
(207) Rossi, G.; Rapallo, A.; Mottet, C.; Fortunelli, A.; Baletto, F.; Ferrando, R. *Phys. Rev. Lett.* **2004**, *93*, 105503.
(208) Darby, S.; Mortimer-Jones, T. V.; Johnston, R. L.; Robert, C. *J. Chem. Phys.* **2002**, *116*, 1536.
(209) Hudgins, R. R.; Imai, M.; Jarrold, M. F.; Dugourd, P. *J. Chem. Phys.* **1999**, *111*, 7865.
(210) Yasuda, H.; Mitsuishi, K.; Mori, H. *Phys. Rev. B* **2001**, *64*, 094101.
(211) Zhang, M.; Efremov, M. Y.; Schiettekatte, F.; Olson, E. A.; Kwan, A. T.; Lai, S. L.; Wisleder, T.; Greene, J. F.; Allen, L. H. *Phys. Rev. B* **2000**, *62*, 10548.
(212) Jiang, Q.; Shi, H. X.; Zhao, M. *J. Chem. Phys.* **1999**, *111*, 2176.
(213) Kwon, K. W.; Lee, H. J.; Sinclair, R. *Appl. Phys. Lett.* **1999**, *75*, 935.
(214) Shi, F. G. *J. Mater. Res.* **1994**, *9*, 1307.
(215) Ouyang, G.; Wang, C. X.; Yang, G. W. *Appl. Phys. Lett.* **2005**, *86*, 171914.
(216) Liang, L. H.; Shen, C. M.; Chen, X. P.; Liu, W. M.; Gao, H. J. *J. Phys.: Condens. Matter* **2004**, *16*, 267.
(217) Schwarz, S. M.; Kempshall, B. W.; Giannuzzi, L. A. *Acta Mater.* **2003**, *51*, 2765.
(218) Buffat, P.; Borel, J. P. *Phys. Rev. A* **1976**, *13*, 2287.
(219) Shimizu, Y.; Ikeda, K. S.; Sawada, S. I. *Phys. Rev. B* **2001**, *64*, 075412.
(220) Baletto, F.; Mottet, C.; Ferrando, R. *Phys. Rev. Lett.* **2003**, *90*, 135504.
(221) Weast, R. C. *CRC Handbook of Chemistry and Physics*, 69th ed.; CRC Press: Boca Raton, FL, 1988−1989; p F50.
(222) Available from http://www.webelements.com.

CR900055F